The Great Oxidation from a minimal ocean–atmosphere model

Matthew D. Schwartz[a], David T. Johnston[b]

[a]Department of Physics, Harvard University, Cambridge, MA, USA

[b]Department of Earth and Planetary Sciences, Harvard University, Cambridge, MA, USA

Corresponding author: M. D. Schwartz

ORCID: M. D. Schwartz 0000-0001-6344-693X; D. T. Johnston 0000-0002-2487-1084

October 1, 2026

Abstract

For two billion years Earth's air carried almost no oxygen; today oxygen is a fifth of it. The textbook story is that the rise came in steps, starting with the Great Oxidation 2.4 billion years ago. We then built a minimal ocean–atmosphere model of the transit with every forcing tied to a measured history or stated as a condition. Each input is fixed by data: rate laws and fluxes by published measurements and models, three quantities by the present-day steady state, the epoch at which the oxygen source overtakes its sinks by the dated onset of the transition, and the decline of volcanic outgassing by the Paleoproterozoic glacial record. Its Great Oxidation is not a step but an oscillation entangled with the glaciations: the decline of methane that precedes the rise of oxygen also cools the planet into the first of four glaciations at 2.45 Ga, each about 25 Myr long and separated by ice-free intervals of about 45 Myr, and each returning the air to anoxia under our assumption that oxygen produced beneath the ice is consumed there. Oxygen first passes the sulfur-isotope threshold at 2.35 Ga and becomes permanent at the last deglaciation, 2.22 Ga, a date that follows from the glaciation count and that assumption. The model's third glaciation ends about 20 Myr later than dated ash beds allow, and the model reproduces neither the Lomagundi carbon-isotope excursion nor the paleosol oxygen level after the transit. As a nontrivial check, we computed the CO_2 values inside the transit itself using two published paleosols, from Canada and Finland, finding results consistent with our model.

Highlights

- An O_2–CH_4–CO_2–phosphate–climate model whose inputs are published data or assumptions
- The glaciation count fixes the outgassing exponent to one percent of its prior range
- The modeled Great Oxidation is an oscillation paced by four snowball glaciations
- The third model glaciation ends about 20 Myr later than the Gordon Lake tuffs allow
- Predicted interglacial CO_2 of 53–253 times pre-industrial is testable with paleosols

Keywords: Great Oxidation Event; Paleoproterozoic glaciations; atmospheric methane; mass-independent sulfur isotopes; carbon cycle model; snowball Earth

Main text (Introduction through Conclusions; headings, citations and displayed equations included; abstract, captions, tables and references excluded): 6,431 words. Abstract: 266 words. References in the main list: 67. Figures: 7. Tables: 3.

PRELIMINARY

1 Introduction

Free oxygen, a fifth of the atmosphere today, was almost absent for roughly the first half of Earth's history. The rise of oxygen began early in the Paleoproterozoic with the Great Oxidation Event (Holland, 2002), usually drawn as the first permanent step of a staircase to modern levels (Alcott et al., 2019). Its onset is marked by the disappearance of the mass-independent fractionation of sulfur isotopes (MIF-S, nonzero $\Delta^{33}S$), a photochemical anomaly preserved in sediments only under air with less than about 10^{-5} of the present atmospheric level (PAL) of oxygen (Farquhar et al., 2000; Pavlov and Kasting, 2002).

Dates from the Kola, Kaapvaal and Superior cratons now bracket the transition and place it within an interval of repeated glaciation. On the Kola craton the MIF-S anomaly disappears stratigraphically below the local glacial deposit (Warke et al., 2020), and on the Kaapvaal craton the low-latitude Makganyene diamictite (Evans et al., 1997) interfingers with the Ongeluk lavas, whose age dates that glaciation (Gumsley et al., 2017). Higher in the same succession, the Transvaal Supergroup, the anomaly is lost by 2.33–2.32 Ga (Bekker et al., 2004; Luo et al., 2016), but in more densely sampled sections it returns at least twice and, on that evidence, is

lost permanently only near 2.22 Ga, coincident with the Lomagundi–Jatuli carbon isotope excursion (Karhu and Holland, 1996; Poulton et al., 2021). Four glaciations fall in this interval under the current correlation of the Transvaal with the Huronian Supergroup of Canada, three under an older one (Rasmussen et al., 2013). The Great Oxidation is therefore increasingly interpreted as a climate-paced transition rather than a single step (Uveges et al., 2023).

Photochemical models established that oxygen and methane destroy each other (Pavlov and Kasting, 2002; Kasting, 2013), and because methane also warmed the Archean Earth, its loss could freeze the planet; in some scenarios oxygen rose first (Pavlov et al., 2000; Kopp et al., 2005) and in others methane collapsed first (Zahnle et al., 2006). In the model of Claire et al. (2006), whose photochemistry and hydrogen escape we adopt, a temperature-dependent biosphere and a parameterized ice–CO_2 switch made methane collapse and recover repeatedly and froze the planet three times (their §7.3). Climate models showed that when the volcanic CO_2 supply cannot prevent glaciation, the planet cycles between glaciated and ice-free states with a period set by the outgassing rate (Tajika, 2007; Mills et al., 2011; Minsky et al., 2026). In those models the outgassing rate was an input and most lacked oxygen chemistry, while the chemical models took the date of the rise from the rock record, as we do. Coupled models have also produced repeated returns to anoxia under imposed forcing (e.g., Alcott et al., 2026) or made deglaciation the trigger of the rise (Harada et al., 2015; Laakso and Schrag, 2017). None of these models has been driven through the transition by dated input histories alone and compared with the dated glacial and $\Delta^{33}S$ records. The outgassing law that such a model requires (Krissansen-Totton et al., 2018) leaves undetermined how steeply volcanic outgassing declines.

In this paper we couple the oxygen–methane chemistry to the carbon cycle and ice in a minimal ocean–atmosphere model with four reservoirs (oxygen, methane, carbon dioxide, phosphate) and an ice state, assembled from published components. Its inputs are dated histories (continental emergence, solar brightening, the volcanic hydrogen supply dated by nickel in iron formations, and organic burial from carbon isotopes), the modern oxygen budget (Holland, 2002) and the assumptions in Table 1. We prescribe two Paleoproterozoic dates: the epoch when the oxygen source first exceeds its sinks, within the age constraints on the onset of the Great Oxidation, and the end of continental emergence, at the first glaciation. Given the other inputs, the glacial record fixes the steepness of the outgassing decline, since at least one Paleoproterozoic snowball glaciation and none after 2.22 Ga confine it to six percent of its published range, and at least four glaciations to one percent. The number and spacing of the glaciations and the date of the last deglaciation therefore belong to the calibration, and we do not offer them as tests. In the model the loss of the last methane triggers the first of four glaciations, the air under each ice cover is anoxic by assumption, and oxygen exceeds the MIF-S threshold in the later interglacials and permanently only from the last deglaciation. We compare this chronology with the dated glacial deposits, the $\Delta^{33}S$ compilation and the oxygen and CO_2 proxies. For the network of Alcott et al. (2019), in which internal feedbacks convert a smooth decline in the reductant input into oxygenation steps, we also determine all steady states at the reductant input of its Great Oxidation and at the weakest burial feedbacks its authors consider (Section 5.1), and likewise for the two-state model of Goldblatt et al. (2006).

2 A minimal ocean–atmosphere model

The model follows four reservoirs (atmospheric oxygen O, methane N and carbon dioxide C, and dissolved marine phosphate P) and an ice state, open water or global glaciation (Fig. 1; Table 1). We integrate them as one system from 3.0 Ga to the present.

2.1 Reservoirs, forcings and their histories

Molybdenum isotopes record shallow-marine oxygen, and hence oxygenic photosynthesis, by 2.95 Ga (Planavsky et al., 2014a), when the model's oxygen source switches on; the contested late-Archean "whiff" of oxygen (Anbar et al., 2007; Slotznick et al., 2022) enters only as a bracket on which nothing in the model rests (Supplementary Text S2). We date the late-Archean decline of the oxygen-consuming volcanic gases with the nickel-to-iron ratio of banded iron formations, which falls from about 2.7 Ga, a decline its compilers attribute to a cooling mantle (Konhauser et al., 2009, 2015). Of the mantle-cooling reading the model keeps only the weaker statement that the series is one of what should be several geochemical proxies of that cooling and of the volcanic hydrogen supply that declines with it, nickel being the one with a compiled marine record, and it reads abundant Archean nickel as saying only that methanogenesis need not have been nickel-limited (a framing we owe to D. T. Johnston).

Shale oxygen isotopes (Bindeman et al., 2018) and the shift toward subaerial volcanism (Kump and Barley, 2007) date continental emergence to the Archean–Proterozoic boundary. In the model, continental weatherability rises linearly from $f_w = 0.5$ at 2.55 Ga to one at 2.45 Ga. This completion date, prescribed

PRELIMINARY

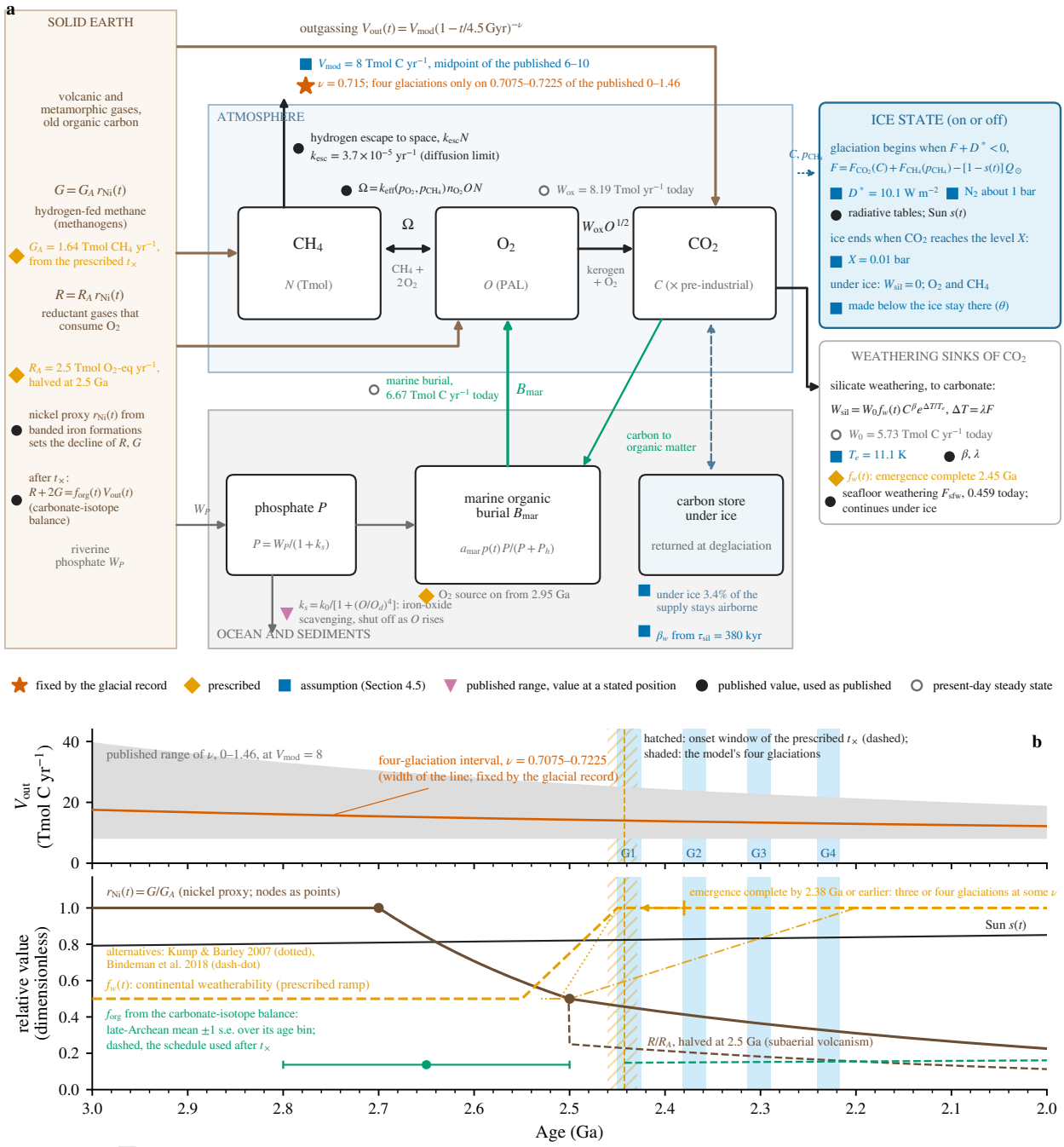

Figure 1: Schematic of the model (four reservoirs and an ice state) and its dated forcing histories. (a) Methane N, oxygen O, carbon dioxide C and ocean phosphate P with every flux in equations (1)–(9) and its value. The symbol beside each input, defined in the legend, marks how that input enters the model (Table 1). (b) Forcing histories on one age axis: outgassing for values of the exponent ν in the four-glaciation interval (line) and across its whole published range (gray), the nickel proxy r_{Ni}, the continental weatherability f_w (with two published alternative emergence histories), solar luminosity $s(t)$ and the organic burial fraction f_{org} derived from carbon isotopes. The tick at 2.38 Ga marks the latest completion of emergence at which some ν gives three or four glaciations. Only ν is fixed by the glacial record; the emergence date and $t_\times$, the epoch at which the oxygen source first exceeds its sinks, are prescribed.

Table 1: Inputs of the model and how each enters. Each is a published value used as published, a quantity fixed by the present-day steady state ($O = 1$, $C = 1$, today's organic burial), a prescribed date or amplitude, an assumption or, for ν alone, a value fixed by the glacial record (Section 2.4). The assumptions are values within published ranges, and the sub-range of each in which three or four Paleoproterozoic glaciations occur at some ν is given in Section 4.5. Last column: published estimates (Holland, 2002; Krissansen-Totton et al., 2018); present-day rows agree by construction or are inputs, so they are not tests. Fluxes in Tmol yr^{-1}, O in PAL, C in multiples of pre-industrial CO_2; details in Supplementary Texts S1 and S2.

Symbol	Meaning	Value (unit)	Source	How it enters	Published comparator
Oxygen, methane and the reductant budget, equations (1)–(4)					
k_{esc}; k_{eff}	hydrogen escape with CH_4; net destruction of CH_4 by O_2	3.7×10^{-5} yr^{-1}; their Fig. 3, interpolated in $\log p_{O_2}$ and $\log p_{CH_4}$	Claire et al. (2006), eq. 12 and Fig. 3	published values; the H_2 freed as water oxidizes the carbon left behind is assumed to escape as well (Suppl. Text S1)	
a_{mar}	marine organic burial today	6.67 Tmol C yr^{-1}	Holland (2002)	present-day steady state	total burial 10.0 ± 3.3
N_A; f_A; t_{ref}	Archean net burial $f_A V_{out}(t_{ref})$	2.07 Tmol C yr^{-1}; 0.137 ± 0.011; 2.65 Ga	Krissansen-Totton et al. (2015)	published value; t_{ref} at the bin midpoint	
W_{ox}	oxidative weathering, $W_{ox} O^{1/2}$	8.19 Tmol yr^{-1} at $O = 1$	law of Laakso and Schrag (2014)	present-day steady state	C oxidation 7.5 ± 2.5 ($+0.27\ \sigma$)
R_A	reductant sink at $r_{Ni} = 1$	2.5 Tmol O_2-eq yr^{-1}, halved at 2.5 Ga	step: Kump and Barley (2007)	prescribed	
G_A	hydrogen-fed methane at $r_{Ni} = 1$	1.64 Tmol CH_4 yr^{-1} (6.56 Tmol H_2 yr^{-1})	$B_{mar} = R + 2G$ at $t_\times$	follows from the prescribed $t_\times$	volcanic H_2 today 4.8 ± 3.6; Archean 8 (Zahnle et al., 2006)
$t_\times$	epoch when the O_2 source first exceeds its sinks	2.44 Ga (2.4425 as integrated), inside 2.46–2.43	Gumsley et al. (2017); Warke et al. (2020)	prescribed; dates move $\leq$9 Myr across the window	
$f_{org}(t)$; δ_{in}	burial fraction after $t_\times$; input $\delta^{13}C$	$f_\times = 0.148$; 0.179 at 1.40 Ga; 0.228 at 0.27 Ga; -5 ± 1 per mil	Krissansen-Totton et al. (2015)	published values; later $\delta^{13}C$ is an input returned	
Carbon dioxide, climate and ice, equations (5)–(9)					
V_{mod}	outgassing today	8 Tmol C yr^{-1}	Krissansen-Totton et al. (2018)	assumption: midpoint of the published range	6–10
ν	outgassing-decline exponent	0.715; four glaciations on 0.7075–0.7225 (1.0% of the range; to 0.7388 with the older count of three)	range: Krissansen-Totton et al. (2018)	fixed by the glacial record	0–1.46, no preferred value
W_0	silicate weathering today	5.73 Tmol C yr^{-1}		present-day steady state	
β; λ	weathering exponent; warming per unit forcing	0.3; 0.69 K (W m^{-2})$^{-1}$	Krissansen-Totton et al. (2018); Byrne and Goldblatt (2014)	published values	β in 0.1–0.5
T_e	weathering e-folding temperature	11.1 K	conventional 5–15 K (Suppl. Text S1)	assumption: within range (glaciations kept for 6.6–19.6 K)	10–40 in Krissansen-Totton et al. (2018)
τ_{sil}; β_w	weathering response time; ocean–air carbon partition	380 kyr; 29.6	Colbourn et al. (2015)	assumptions: slow end of 170–380 kyr; modern β_w applied at all CO_2 (Sec. 4.5)	
F_{sfw}; n	seafloor weathering; heat-flow exponent	$F_d = 0.459$ Tmol C yr^{-1}, $E_a = 75$ kJ mol^{-1}; 0.73	Krissansen-Totton and Catling (2017)	published medians; n at the upper end (no effect on the glaciations)	
F; p_{N_2}; $Q_\odot$	radiative forcing; nitrogen; sunlight, Sun $s(t)$	line-by-line tables; 1 bar; 238.17 W m^{-2}	Byrne and Goldblatt (2014); Gough (1981)	published; p_{N_2} an assumption (glaciations kept down to 0.57 bar)	
D^*	forcing deficit at which ice advances	10.1 W m^{-2}	Voigt et al. (2011)	assumption: lowest published (glaciations kept up to 14.7)	17.9–30.2; 15.8 (Feulner et al., 2023)
X; r, s_{cal}, Q_{ice}	CO_2 at which ice retreats; rule constants	0.01 bar (36 × pre-industrial); 0.686, 0.94, 136.1 W m^{-2}	Abbot et al. (2012); Hoffman et al. (2017)	X an assumption: low end of 0.01–0.1 bar; rest published	
θ; β_{ice}	sub-ice venting; sub-ice carbon partition	none vented; $\beta_{ice} = \beta_w$: 3.4% airborne, up to 3.1×10^{20} mol C per glaciation stored (no identified carrier) and returned at deglaciation; this store, D^* and p_{N_2} are the largest physical assumptions	Hoffman et al. (2017); Le Hir et al. (2008); Suppl. Text S1	assumptions; glaciations kept for θ up to a tenth (four at $\nu = 0.715$ with $\theta \leq 0.03$); Marinoan 5.1 vs 4–15 Myr	
Forcing histories (Fig. 1b) and later schedules					
$r_{Ni}(t)$	banded-iron-formation Ni/Fe, normalized	unity to 2.7 Ga, 0.5 at 2.5, 0.0225 at 0.55 Ga, log-linear	Konhauser et al. (2009, 2015)	published series (shape and timing)	
$f_w(t)$; O_2 source	continental emergence; photosynthesis on	0.5 at 2.55 to unity at 2.45 Ga; on from 2.95 Ga (the contested 2501 ± 8-Ma whiff enters as a bracket only)	Kump and Barley (2007); Planavsky et al. (2014a)	prescribed dates (glaciations kept if complete by 2.38 Ga)	2.50–2.20 Ga (Bindeman et al., 2018)
k_0; W_P; $p(t)$; L_0	phosphate trap and delivery; productivity; land plants	Archean trap $k_0 = 10$; later schedules between 0.75 and 0.40 Ga (Suppl. Text S1)	Suppl. Text S1	prescribed; no effect on the glaciations ($k_0 = 4$ or 60 keep four)	
$S(0)$; net burial	O_2-independent sink and net organic burial today	1.82 Tmol O_2-eq yr^{-1}; 1.82 Tmol C yr^{-1} ($O = 1$, $C = 1$ by construction)	eq. (4)	inputs returned, not tests	2.4 ± 1.8 ($-0.32\ \sigma$); net 2.5 ± 1.0 or 1.2 ± 0.8

PRELIMINARY

at the onset of Paleoproterozoic glaciation in the rock record, sets the date of the model's first glaciation.

2.2 Oxygen, methane and the reductant budget

With fluxes in Tmol yr^{-1}, t the age and dots denoting rates of change forward in time, atmospheric oxygen grows by marine organic burial and falls by methane oxidation, by weathering of old organic carbon and by reduced volcanic and metamorphic gases,

$$n_{O_2}\,\dot{O} = B_{\mathrm{mar}} - 2\,\Omega - W_{\mathrm{ox}}\,O^{1/2} - R(t), \qquad O > 0. \tag{1}$$

Methane is produced by methanogens from volcanic hydrogen and lost to oxidation and to escape of its hydrogen to space,

$$\dot{N} = G(t) - \Omega - k_{\mathrm{esc}}N, \qquad \Omega = k_{\mathrm{eff}}(p_{O_2}, p_{CH_4})\,n_{O_2}\,O\,N. \tag{2}$$

Here O is in units of the present atmospheric level (PAL, $n_{O_2} = 3.7 \times 10^{19}$ mol), N in Tmol with $p_{CH_4} = N/N_{\mathrm{atm}}$ in bar, and the omitted land-biosphere terms (Supplementary Text S1) vanish before land plants. The oxidation Ω consumes two O_2 per CH_4, with k_{eff} the effective rate constant of Claire et al. (2006) for the net photochemical destruction of CH_4 by O_2, and $k_{\mathrm{esc}}N$ their diffusion-limited escape of the hydrogen carried by methane. In anoxic air, water oxidizes the carbon left behind and frees an equal amount of hydrogen, which we assume also escapes; if methanogens consume it instead (Kharecha et al., 2005), Archean methane doubles (hereafter the methane-only case) and no glaciation or oxygen date moves more than 2.7 Myr (Supplementary Text S1).

Marine organic burial, $B_{\mathrm{mar}} = a_{\mathrm{mar}}\,p(t)\,P/(P{+}P_h)$, is a productivity factor times a saturating dependence on phosphate, and in the Archean equals the net organic burial implied by the carbon isotope record, $N_A = 2.07$ Tmol C yr^{-1} (Krissansen-Totton et al., 2015). Oxidative weathering follows the square-root law of Laakso and Schrag (2014), with W_{ox} and a_{mar} fixed by the present-day steady state.

The sink $R(t) = R_A\,r_{\mathrm{Ni}}(t)$ is the outgassing/mantle-cooling forcing, dated via the Ni proxy (in the equations, the reductant sink riding the measured nickel decline and the emergence step), with r_{Ni} the normalized nickel series and R_A a prescribed amplitude, halved at the shift toward subaerial volcanism (Table 1). The methane source $G(t) = G_A\,r_{\mathrm{Ni}}(t)$ follows the same series, which dates the decline of a single volcanic hydrogen supply, of which G is the part methanogens convert to methane and R the remainder, so that the fall of G is a hydrogen famine rather than a nickel famine and nickel enters no equation as a nutrient. Requiring the open-water oxygen budget to cross zero at a prescribed epoch $t_\times$ within the dated onset window of the Great Oxidation, 2.46–2.43 Ga,

$$B_{\mathrm{mar}} = R(t_\times) + 2\,G(t_\times), \qquad t_\times = 2.44\ \mathrm{Ga} \quad \text{(prescribed)}, \tag{3}$$

gives $G_A = 1.64$ Tmol CH_4 yr^{-1}. The model computes no crossing epoch of its own; $t_\times$ enters only through G_A.

Until 2.64 Ga the sink R alone, in oxygen equivalents, exceeds the oxygen supplied by burial, so the air holds no free oxygen and the unoxidized part of R is also converted to methane; equations (1) and (2) then become

$$O = 0, \qquad \dot{N} = G + \tfrac{1}{2}\,(R - B_{\mathrm{mar}}) - k_{\mathrm{esc}}N \qquad (R > B_{\mathrm{mar}}), \tag{2′}$$

and in steady state, hydrogen escape removes the whole excess of reductant supply over burial, $2k_{\mathrm{esc}}N = R{+}2G{-}B_{\mathrm{mar}}$, the anoxic balance of Claire et al. (2006) under our escape assumption. Under ice that excess is counted as hydrogen lost to space (Supplementary Text S1).

After $t_\times$ the sink $S = R + 2G$ no longer follows the nickel series, and we set it to the net organic burial that the carbon isotope mass balance implies for the model's outgassing V_{out},

$$S(t) = R + 2G = f_{\mathrm{org}}(t)\,V_{\mathrm{out}}(t), \qquad t < t_\times, \tag{4}$$

with the organic burial fraction f_{org} interpolated between its value at $t_\times$ and the later-era means of Krissansen-Totton et al. (2015), and R/G held at its value at $t_\times$ (alternatives in Supplementary Text S1).

Phosphate relaxes quickly to $P = W_P/(1{+}k_s)$, with W_P the riverine delivery (not scaled with continental emergence, a simplification) and k_s the scavenging onto iron oxides until deep-water oxygen passes a threshold (Table 1). The Archean scavenging strength does not affect the glaciations, Archean burial being held at N_A through $p(t)$, and is bounded by the phosphorus budget of Laakso and Schrag (2017) (Supplementary Text S6).

PRELIMINARY

2.3 Carbon dioxide, climate and ice

On the open-water branch atmospheric CO_2 grows by outgassing and oxidative weathering and falls by organic burial, by continental silicate weathering W_{sil} and by seafloor weathering F_{sfw}, the low-temperature carbonation of ocean crust (Krissansen-Totton and Catling, 2017),

$$n_{\mathrm{C}}\,\beta_w\,\dot{C} = V_{\mathrm{out}}(t) + W_{\mathrm{ox}}O^{1/2} - B_{\mathrm{mar}} - W_{\mathrm{sil}} - F_{\mathrm{sfw}}, \tag{5}$$

where C is in multiples of the pre-industrial level, n_{C} the carbon in one such atmosphere and β_w the ocean–atmosphere carbon, in atmospheres, that moves with each atmosphere of CO_2 (Table 1). Outgassing follows Krissansen-Totton et al. (2018),

$$V_{\mathrm{out}}(t) = V_{\mathrm{mod}}\left(1 - \frac{t}{4.5\ \mathrm{Gyr}}\right)^{-\nu}, \tag{6}$$

where V_{mod} is the modern flux and ν (which they sampled over $[0, 1.46]$ with no preferred value) is the quantity the glacial record fixes: a larger ν means more early volcanic CO_2 and, over the upper part of that range, fewer glaciations. Silicate weathering is

$$W_{\mathrm{sil}} = W_0\,f_w(t)\,C^{\beta}\exp(\Delta T/T_e), \qquad \Delta T = \lambda F, \tag{7}$$

with W_0 fixed by $C = 1$ today, f_w the continental weatherability, ΔT the warming from the forcing F at climate sensitivity λ, T_e a conventional e-folding temperature and β a published exponent (Table 1).

Climate enters through the radiative forcing F relative to the pre-industrial state, and the open-water branch ends when F falls below a threshold,

$$\begin{aligned} F(C, p_{\mathrm{CH_4}}, t) &= F_{\mathrm{CO_2}}(C) + F_{\mathrm{CH_4}}(p_{\mathrm{CH_4}}) - [1 - s(t)]\,Q_{\odot}, \\ F + D^* &< 0 \quad \text{(glaciation begins)}, \end{aligned} \tag{8}$$

where $F_{\mathrm{CO_2}}$ and $F_{\mathrm{CH_4}}$ are interpolated from the line-by-line forcings of Byrne and Goldblatt (2014) with one bar of nitrogen. The last term is the deficit in sunlight from the fainter young Sun, with $Q_{\odot}$ the sunlight absorbed today and $s(t)$ the relative solar luminosity (Gough, 1981). The threshold D^* is the deficit at which the general circulation model of Voigt et al. (2011) runs away to global ice cover, the most glaciation-prone value published (Table 1).

A glaciation persists until CO_2, with any methane, reaches the far higher deglaciation level of the general circulation models compared by Abbot et al. (2012), set at the low end of the proxy range of Hoffman et al. (2017). During a glaciation continental weathering stops, outgassing continues, and cold seafloor weathering at the freezing point T_{f} removes about 10–11% of the outgassed carbon,

$$n_{\mathrm{C}}\,\beta_{\mathrm{ice}}\,\dot{C} = V_{\mathrm{out}}(t) - F_{\mathrm{sfw}}(C, T_{\mathrm{f}}, t), \qquad \beta_{\mathrm{ice}} = \beta_w. \tag{9}$$

Under this sub-ice carbon rule a fraction $1/\beta_{\mathrm{ice}} = 3.4\%$ of the remainder stays airborne, and the rest, up to 3.1×10^{20} mol of carbon per glaciation, 99 times the present ocean's dissolved inorganic carbon, enters a store that is returned at deglaciation and weathered away over the following interglacial. This exchangeable store is, with the glaciation threshold and the nitrogen inventory, the model's largest physical assumption. The model has no dissolved-inorganic-carbon or alkalinity variable, and we have identified no carrier that would hold and return that much carbon (Supplementary Text S1). We also assume that oxygen and methane produced beneath the ice are consumed there, so that the air stays anoxic and methane-free throughout a glaciation (the sub-ice treatment; Supplementary Text S1).

2.4 Inputs and the outgassing exponent

Most inputs in Table 1 are measurements or published laws, and three are fixed by the present-day steady state. The epoch $t_{\times}$, the emergence and photosynthesis dates, R_A and the post-Paleoproterozoic schedules are prescribed (Fig. 2). Eight are assumptions, values chosen within a published range. The model's Paleoproterozoic glaciations and their anoxia depend chiefly on five of them (D^*, about one bar of nitrogen, T_e, the sub-ice carbon rule with its exchangeable store, and the consumption of oxygen and methane beneath the ice). Seven of the eight were set without reference to the Paleoproterozoic record. The eighth, the sub-ice carbon rule, was preferred to an alternative partly because four glaciations occur with it, and the glaciation count therefore calibrates that rule together with ν (Supplementary Text S1).

With the other inputs fixed at their Table 1 values, a snowball glaciation (the low-latitude Makganyene) requires $\nu < 0.7975$ (0.839 in the methane-only case), and the absence of glaciation between 2.22 Ga and the Cryogenian requires $\nu > 0.7075$, confining ν to 6.2% (9%) of its published range. The model has at least four

PRELIMINARY

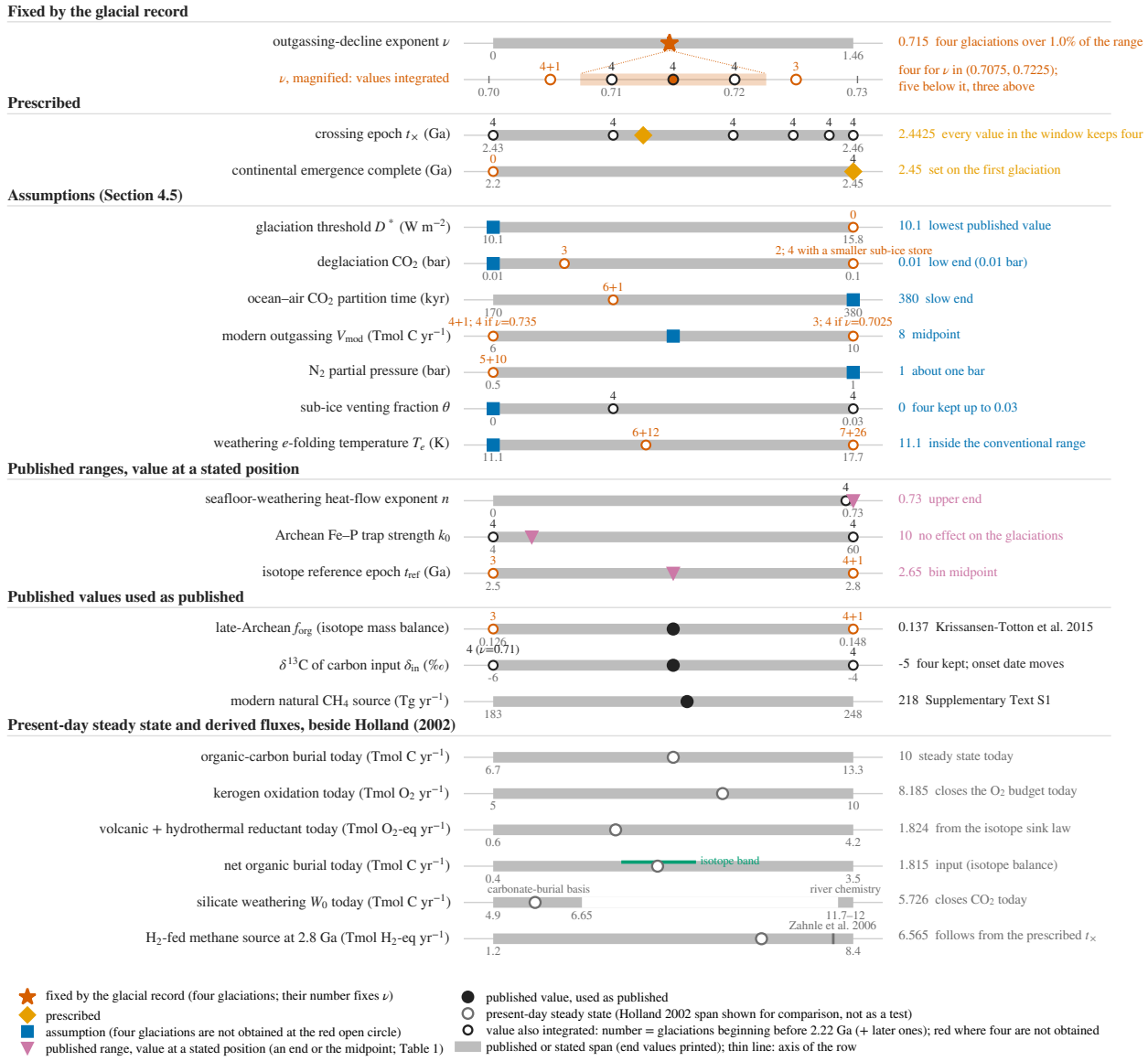

Figure 2: Model inputs on their published ranges. Of the inputs plotted, only the outgassing exponent ν is fixed by the glacial record with which the model is compared. Each row shows the range of one input (gray bar), the value used (symbol) and the other values at which the model was integrated (open circles). The open circles are labeled with the number of glaciations beginning before 2.22 Ga (and, after a plus sign, the number beginning later) and are drawn in red unless four begin before that date and none later. A magnified strip below the ν row shows the four-glaciation interval 0.7075–0.7225 (shaded, 1.0% of the range sampled by Krissansen-Totton et al. (2018)), computed with the other inputs at the values used, and the number of glaciations at neighboring values of ν. For an input other than ν, the numbers at its open circles are obtained by changing that input alone, with the remaining inputs, including ν, held at their Table 1 values. Where a number was instead obtained at another value of ν, that value is printed beside the number. The sub-ranges of the assumptions within which three or four glaciations occur at some ν are given in Section 4.5. Present-day rows are shown beside the estimates of Holland (2002) for comparison only.

glaciations by 2.22 Ga (the minimum under the current Transvaal–Huronian correlation) and none later only for $0.7075 < \nu < 0.7225$, 1.0% of the range, where it has exactly four (Supplementary Text S4). Admitting the three glaciations of the older correlation widens the interval to 2.1% of the range, and throughout that interval the transition is oscillatory.

Because ν is fixed by the number of glaciations, that number is part of the calibration, and so are their spacing, the length of the third interglacial and the date of the last deglaciation, at which, given the sub-ice treatment, oxygen becomes permanent in the model. We offer none of these as agreement; Table 2 marks which statements follow from the glaciation count. We specified the comparisons of Section 4, their dated bounds and the values expected of the model before the integrations reported here, using earlier integrations of the same equations, and did not adjust them afterward. Supplementary Text S3 lists them, including those the model fails, and the later exploratory calculations.

3 Geological constraints

We use the dated beds and atmospheric proxies as one-sided bounds, taking each age at the 2σ limit that makes its bound weaker. A bed beneath a diamictite gives a maximum age for the onset of glaciation, a lava within it dates the ice, and a bed above it gives a minimum age for deglaciation.

3.1 Dated glacial deposits

Figure 3 shows the dated units by craton (sources in Supplementary Text S3). On the Kaapvaal craton the Ongeluk lavas (2425.5 ± 2.6 Ma) interfinger with the upper part of the Makganyene diamictite (Gumsley et al., 2017), which overlies Heynskop Formation (Koegas Subgroup) beds no older than 2451.5 ± 2.5 Ma (Senger et al., 2023). Gordon Lake tuffs above the Huronian Gowganda diamictite (Rasmussen et al., 2024) and the basal Timeball Hill shale in the Transvaal (Hannah et al., 2004) require the third glaciation to have ended by 2.310 Ga. Upper Timeball Hill tuffs beneath the Rietfontein diamictite give a maximum age for the start of the fourth glaciation (Rasmussen et al., 2013), and only an age model for the overlying Hekpoort lava dates its end (Schröder et al., 2016). We adopt the current Transvaal–Huronian correlation of Gumsley et al. (2017), which gives four glaciations across the cratons, a minimum because preservation is incomplete. An alternative correlation within the Transvaal basin, with a single Duitschland–Rooihoogte unit and a unidirectional loss of the MIF-S anomaly (Havsteen et al., 2023; Beukes and Schröder, 2024), also gives four (Fig. 3).

3.2 The sulfur isotope record

Figure 4 shows the 1,689 Transvaal $\Delta^{33}S$ measurements compiled by Uveges et al. (2023), clustered at a few dated ages, and the intervals in which the model atmosphere permits the anomaly. Its preservation requires low oxygen and possibly also methane above about 8 ppmv (Zahnle et al., 2006), and we use both criteria; under either, absence of the anomaly is necessary but not sufficient evidence of oxygenated air (Halevy et al., 2010). Averaged in 5-Myr bins, the compilation changes between anomaly-bearing and anomaly-free states 3 times on the re-dated Koegas Subgroup chronology (Senger et al., 2023). Synthetic histories sampled at the compilation's ages, with each dated unit moved as a whole within its age limits, show that this reversal count cannot distinguish one oxic–anoxic cycle from six, nor exclude a single loss of the anomaly with no return for most dates of that loss (Fig. 4b; Supplementary Text S3). The evidence that the anomaly returned is therefore stratigraphic, within single cores (Poulton et al., 2021), and we test the model against the dated sample clusters.

Exposure of and access to rocks that capture the transition are limited, so progress in this field has generally come from new measurements on the same drill cores and sections that earlier studies used. The single-step loss of the anomaly (Bekker et al., 2004) and its later returns (Poulton et al., 2021; Uveges et al., 2023) were both identified in one core, EBA-2, at overlapping depths. The two readings differ in sampling density, not in rocks; that is the ordinary condition of a field with few sections, and it means that independent confirmation is scarcer here than the citation record suggests, for the reversal counts in this paper as much as for any published position.

3.3 Oxygen and carbon dioxide proxies

Detrital uraninite and pyrite from the first Huronian interglacial limit contemporaneous atmospheric oxygen to less than 1.53×10^{-4} PAL (Johnson et al., 2014). Iron retention in paleosols requires at least 0.14 PAL by 2.2–2.0 Ga (Rye and Holland, 1998), although the weathering barometer of Kanzaki and Murakami (2016) allows far lower values; one chromium isotope estimate caps mid-Proterozoic oxygen at 10^{-3} PAL (Planavsky

PRELIMINARY

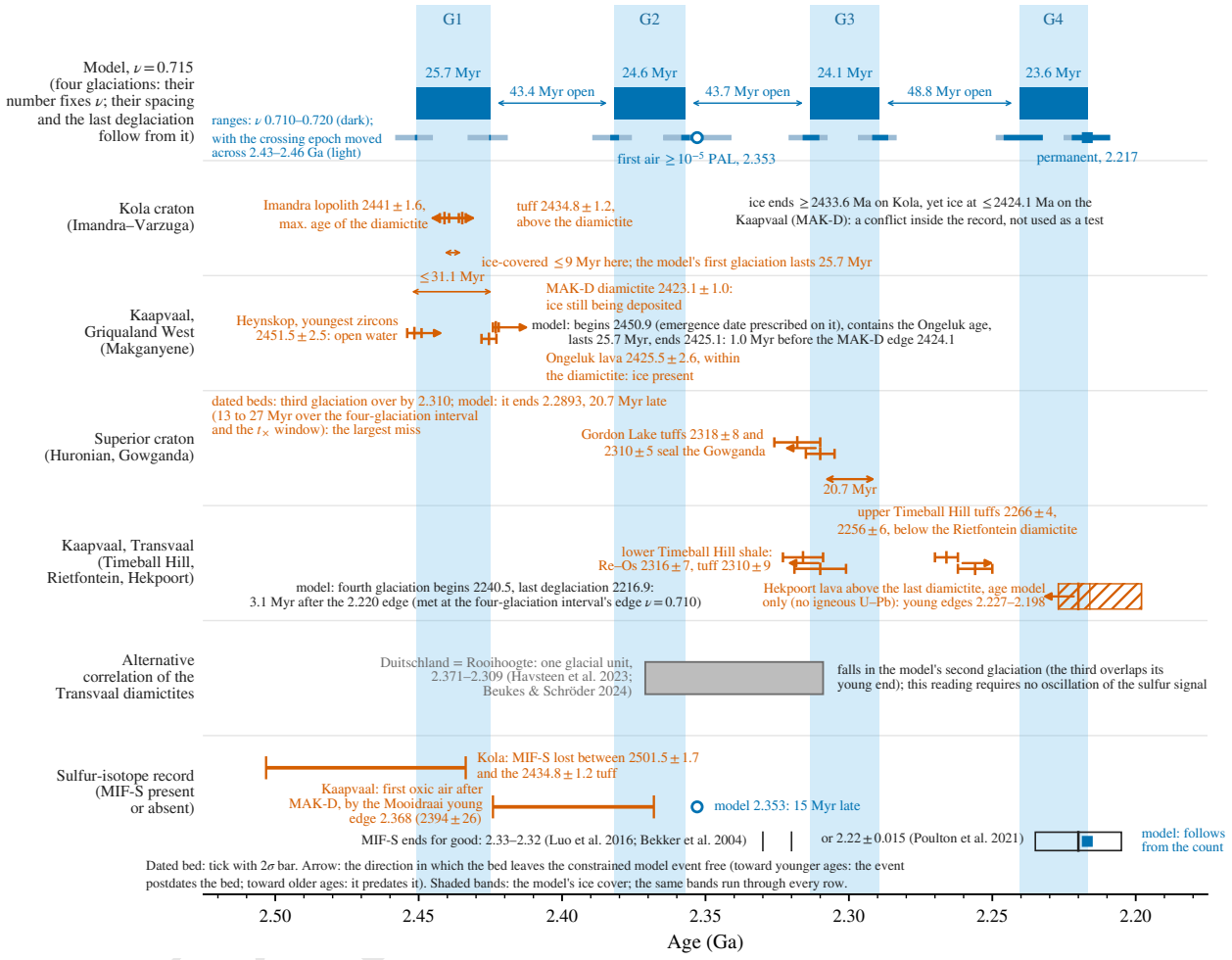

Figure 3: The model's four glaciations (bands at $\nu = 0.715$, durations and gaps printed) against the dated units (ticks with 2σ bars, arrows toward the ages each allows; Section 3.1). The first glaciation, whose start is prescribed, spans the Ongeluk lava age, and the fourth postdates the upper Timeball Hill tuffs; the third ends 20.7 Myr later than the Gordon Lake tuffs allow, which is the model's largest discrepancy with the dated units and depends on the adopted sub-ice carbon store (Table 3). Whiskers: ranges over the four-glaciation interval of ν (dark) and with $t_\times$ also varied across the onset window (light). Hatched: the Hekpoort age model; gray box: the age range of the single basal diamictite in the alternative Transvaal correlation (Havsteen et al., 2023; Beukes and Schröder, 2024). Bottom: age constraints from the sulfur isotope record beside the model's date of first oxic air and its date of permanent oxygenation, which is set by the number of glaciations and by the sub-ice treatment, and is not a test.

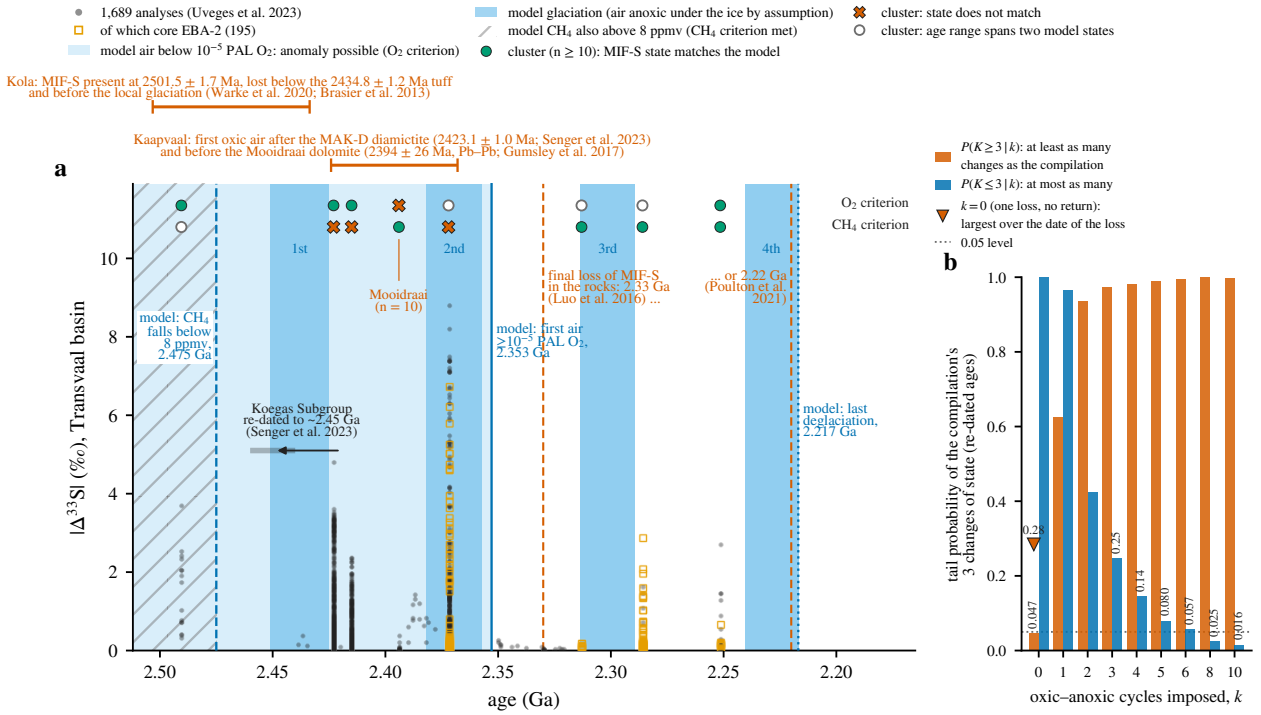

Figure 4: The Transvaal $|\Delta^{33}S|$ compilation and the intervals in which the model's atmosphere permits the anomaly under two criteria. (a) The 1,689 analyses compiled by Uveges et al. (2023), core EBA-2 distinguished. Shaded intervals have model oxygen below 10^{-5} PAL (Pavlov and Kasting, 2002), before 2.353 Ga and during each later glaciation; in the hatched interval, which ends at 2.475 Ga (2.458 Ga in the methane-only case of Section 2.2), model methane is also above 8 ppmv (Zahnle et al., 2006). Symbols mark the dated sample clusters ($n \geq 10$) under each criterion as matched by the model (filled circles), mismatched (crosses) or undetermined because the cluster's age range spans two model states (open circles). Brackets show the Kola and Kaapvaal constraints on the onset of oxygenation. Orange dashed lines are the two estimated ages of the final loss of the anomaly (Luo et al., 2016; Poulton et al., 2021); the arrow marks the shift of the Koegas Subgroup samples to their older re-dated age (Senger et al., 2023; Supplementary Text S3). (b) Binned at 5 Myr on the re-dated chronology, the compilation changes between anomaly-bearing and anomaly-free states 3 times. Bars give the probability that a synthetic history with k oxic–anoxic cycles at random positions through the transition shows at least as many changes as the compilation (orange) or at most as many (blue), from 20,000 histories per k sampled at the compilation's ages with one age draw per dated unit and stratigraphic order kept. For a single loss with no return ($k = 0$) the orange bar is averaged over the date of the loss and the triangle marks its largest value. The model's anoxic first interglacial and its date of first oxic air are tested against the dated clusters in (a). In (b) no history with one to six cycles is rejected at the 0.05 level (dotted line), a single loss with no return is rejected only for some dates of the loss, and histories with eight or ten short cycles are rejected at that level ($P = 0.025$ and 0.016, respectively), so the number of changes of state in the compilation does not measure the number of oxic–anoxic cycles.

et al., 2014b). The two paleosol CO_2 barometers differ by an order of magnitude across the transition: mass balance gives 10–50 times the pre-industrial level for Neoarchean profiles (Sheldon, 2006; Driese et al., 2011), and porewater inversion gives 160–490 times for profiles formed just before the first glaciation (Kanzaki and Murakami, 2015).

4 Results

Results are given at the principal value $\nu = 0.715$, the midpoint of the four-glaciation interval, with ranges over the wider interval (three or four glaciations) that the glacial record allows.

4.1 An oscillatory transition paced by glaciations

In the late Archean the model atmosphere contains negligible oxygen and about 279 ppmv of methane (Fig. 5). As the volcanic hydrogen supply declines and the continents emerge, methane falls to 4.4 ppmv by 2.46 Ga, and the first glaciation begins at 2.451 Ga (8.4 Myr before the crossing epoch $t_\times$), a date set by the prescribed completion of emergence. Methane drops below ten ppmv 30.5–31.9 Myr before the first ice (12 Myr in the methane-only case). The glaciation is triggered by the last stage of the methane collapse of Zahnle et al. (2006) and Claire et al. (2006) acting on a climate that continental weathering has already cooled nearly to the glaciation threshold. Carbon dioxide at entry is 0.93 of the level at which the climate would glaciate with no methane, and the loss of the remaining 2.1 ppmv of methane makes up the difference. Across the onset window and the allowed interval of ν the crossing epoch falls within the first glaciation or before it in open water, never after a deglaciation, and the first glaciation shifts by at most 9 Myr from its principal date (Supplementary Text S4). In all these cases oxygen stays under 6.1×10^{-6} PAL until the first glaciation and exceeds the MIF-S threshold only after it.

Under global ice, carbon dioxide accumulates, mostly in the sub-ice store of equation (9), until it reaches the deglaciation level 25.7 Myr after the onset, at 2.425 Ga. The store is returned at the deglaciation, hothouse weathering draws carbon dioxide back down to the glaciation threshold, and the planet glaciates again. We find four glaciations (Fig. 5d–f), each 23.6–25.7 Myr long and separated by interglacials of 43.4, 43.7 and 48.8 Myr that, like the number of glaciations, are fixed by ν and belong to the calibration. These repeated glaciations are the outgassing–weathering limit cycle of Tajika (2007); no periodic forcing is imposed. The glacial era lasts 234 Myr; after the fourth deglaciation the drawdown of carbon dioxide does not reach the glaciation threshold before 2.128 Ga, and thereafter the brightening Sun keeps the warm, methane-free state above that threshold.

In the model the glacial cycle paces the changes in atmospheric oxygen, and oxygen does not drive the glaciations (Fig. 5a,d). The first interglacial is anoxic (at most 4.8×10^{-6} PAL), and each glaciation returns the air to anoxia because oxygen and methane produced beneath the ice are assumed to be consumed there (Section 5.2). Atmospheric oxygen first exceeds the MIF-S threshold of 10^{-5} PAL at 2.353 Ga (4 Myr after the second deglaciation), and each interglacial is more oxic than the last because the isotope-inferred sink $S(t)$ keeps declining while the burial flux stays flat. Oxygen remains above that threshold permanently from the fourth deglaciation (2.217 Ga), which is the last because the glacial record that fixes ν includes the absence of later ice.

4.2 Glacial chronology against the dated successions

The first glaciation, whose start is prescribed, spans the age of the Ongeluk lavas throughout the allowed interval of ν and is 5.4 Myr shorter than the longest duration the Kaapvaal dates allow; neither property follows from the glaciation count (Fig. 3; Table 2). However, the third glaciation ends at 2.289 Ga, 20.7 Myr later than the Gordon Lake tuffs and the diamictite-free lower Timeball Hill shale allow. The discrepancy is 18–44 Myr across the allowed interval of ν and persists throughout the onset window, whether the Duitschland and Rooihoogte diamictites record two glaciations or one. We attribute it to the glaciations' even spacing under the smooth outgassing law (68.3–72.9 Myr from start to start, lengthened by the carbon returned at each deglaciation), whereas the dated beds require closer spacing of the first three (Supplementary Text S3; Table 3). The fourth glaciation begins 21.5 Myr after the upper Timeball Hill tuffs, and the last deglaciation, whose date follows from the glaciation count, falls 3.1 Myr after the youngest age of the Hekpoort age model (Table 2).

4.3 Sulfur isotopes and interglacial oxygen

The sulfur isotope record tests one feature of the model, the anoxic first interglacial followed by oxic air early in the second (Fig. 4), under the two criteria for preserving the MIF-S anomaly, between which the model

PRELIMINARY

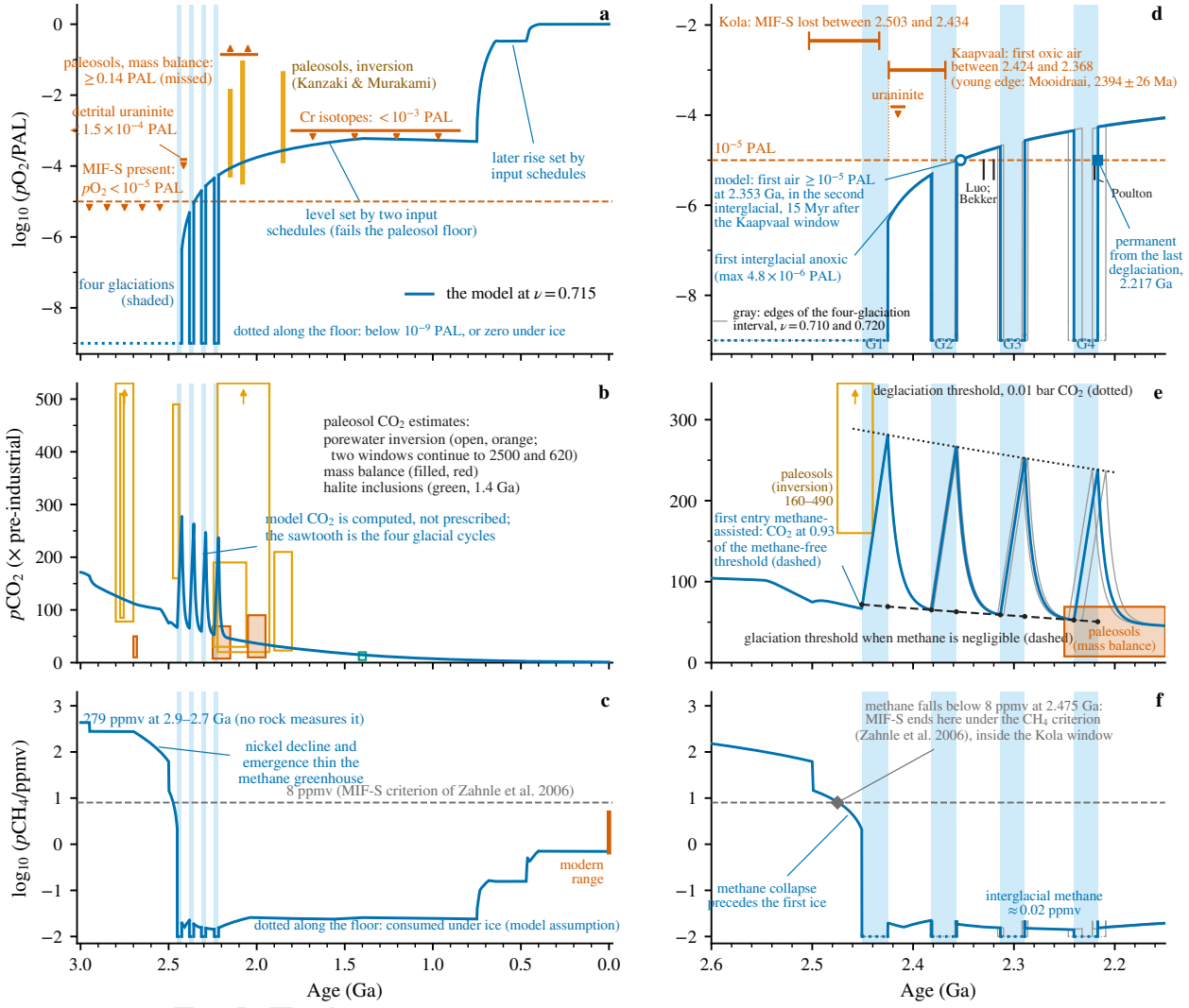

Figure 5: O_2, CO_2 and CH_4 in the model at $\nu = 0.715$ since 3.0 Ga, (a)–(c), and across the Great Oxidation, (d)–(f), with gray curves at the two ends of the four-glaciation interval of ν. As in Section 2.2, the hydrogen freed when water oxidizes methane carbon is assumed to escape; in the methane-only case, in which methanogens consume that hydrogen instead, Archean methane is about twice as high as drawn. Methane collapses before the first glaciation, and the air is anoxic during each glaciation (by assumption, oxygen and methane produced under the ice are consumed there). Oxygen first exceeds 10^{-5} PAL in the second interglacial (2.353 Ga) and stays above it from the last deglaciation (2.217 Ga), a date that follows from the glaciation count and the sub-ice assumption. Red: rock-record bounds; ticks in (d): permanent end of MIF-S at 2.33–2.32 Ga (Luo et al., 2016; Bekker et al., 2004) or 2.22 Ga (Poulton et al., 2021). The later oxygen level in (a) is set by two input schedules, the organic burial flux and the reductant sink inferred from carbon isotopes.

Table 2: Dated statements of the model and the measurements that test them. The first glaciation, whose start is prescribed, spans the Ongeluk lava age, oxygen in the first ice-free interval stays below the detrital-uraninite bound, and the fourth glaciation begins after the upper Timeball Hill tuffs. However, the third glaciation ends 20.7 Myr later than the Gordon Lake tuffs allow (with the adopted sub-ice carbon store; crustal storage in Table 3). Under the oxygen-only criterion the MIF-S anomaly is also lost too late to satisfy the Kaapvaal and Kola constraints on the onset of oxygenation, and under the methane criterion it ends before deposition of the anomaly-bearing Koegas Subgroup and does not return. Model values at $\nu = 0.715$, followed in parentheses by their range over the interval of ν giving three or four Paleoproterozoic glaciations. Bed ages carry 2σ uncertainties; O_2 in units of the present atmospheric level (PAL), CO_2 in multiples of pre-industrial. Rows marked yes follow from fixing ν on the glaciation count and are not support for the model whatever their outcome. Full tables in Supplementary Text S3.

model statement	follows from the glaciation count	measurement that tests it	outcome
First glaciation 2.4509–2.4251 Ga, 25.7 Myr long; entry set by the prescribed emergence date	no	Heynskop maximum depositional age 2451.5 ± 2.5 Ma below; Ongeluk lavas 2425.5 ± 2.6 Ma in the ice; diamictite MAK-D 2423.1 ± 1.0 Ma under ice; hence at most 31.1 Myr (Senger et al., 2023; Gumsley et al., 2017); Kola: at most 9 Myr (Warke et al., 2020)	Ongeluk and Kaapvaal duration met; MAK-D not met by 1.0 Myr, met for $t_\times$ at the young end of its window; Kola not met (Kola and Kaapvaal differ by ≥9.5 Myr within the rock record)
Third glaciation ends 2.289 Ga (2.266–2.292)	no	Gordon Lake tuffs 2318 ± 8, 2310 ± 5 Ma above the last Huronian diamictite (Rasmussen et al., 2024); diamictite-free lower Timeball Hill 2316 ± 7 (Re–Os), 2310 ± 9 Ma (Hannah et al., 2004; Rasmussen et al., 2013): ice gone by 2.310 Ga; a termination age at the Rooihoogte or Gowganda contact would settle it	late by 20.7 Myr (18–44; 13–27 over the four-glaciation interval and the $t_\times$ window); with the sub-ice carbon kept in ocean crust, met by 3.3 or missed by up to 2.0 Myr, depending on ν (Table 3)
Fourth glaciation begins 2.2405 Ga (2.2324–2.2461)	no	upper Timeball Hill tuffs 2266 ± 4, 2256 ± 6 Ma below the Rietfontein diamictite (Rasmussen et al., 2013): entry after 2.262 Ga	met by 21.5 Myr
Last deglaciation 2.217 Ga (2.209–2.283), when oxygen becomes permanent in the model (given the sub-ice treatment)	yes	Hekpoort lava above the Rietfontein, age model only, 2247 ± 20 Ma (Schröder et al., 2016): deglaciation 2.256–2.220 Ga; an igneous U–Pb age would settle it	3.1 Myr young at $\nu = 0.715$, inside at the interval's lower edge
Four glaciations before 2.22 Ga, none after; ice-free intervals 43.4, 43.7, 48.8 Myr; no ice or sulfur anomaly after the last deglaciation	yes	any glacial deposit or mass-independent sulfur younger than 2.22 Ga on the Kaapvaal-correlated frame; Timeball Hill open-marine interval ≥48 Myr (Hannah et al., 2004; Rasmussen et al., 2013)	consistent by construction; listed for completeness, not as support
First ice-free interval (2.4251–2.3818 Ga) anoxic, $O_2 \leq 4.8 \times 10^{-6}$ PAL; no oxidation pulse at Hotazel time	no	detrital uraninite and pyrite of the first Huronian interglacial: $O_2 < 1.53 \times 10^{-4}$ PAL (Johnson et al., 2014; Gumsley et al., 2017); Mn and Ce oxidation in the Hotazel Formation on the Ongeluk lavas (Gumsley et al., 2017)	uraninite bound met; the Hotazel reading not met; a dated redox proxy inside the interval would settle it
Air first passes 10^{-5} PAL at 2.353 Ga (2.348–2.355), 4 Myr after the second deglaciation	no	Kaapvaal: after MAK-D, before the Mooidraai dolomite 2394 ± 26 Ma (whole-rock Pb–Pb; young edge 2.368 Ga; Gumsley et al., 2017); Kola: anomaly lost below the 2434.8 ± 1.2 Ma tuff, before the local ice (Warke et al., 2020; Brasier et al., 2013)	O_2-only criterion (Pavlov and Kasting, 2002): late by 15 Myr (Kaapvaal), 81 Myr (Kola); CH_4 criterion (Zahnle et al., 2006): anomaly ends 2.475 Ga, or 2.458 in the methane-only case, either way inside the Kola window but before the Koegas Subgroup; no return
Anoxic first interval and later returns to anoxia recorded in a second basin	no	Huronian Supergroup: sulfur isotope and redox proxies from the Mississagi to the Gordon Lake formations; detrital pyrite and uraninite above each diamictite (Gumsley et al., 2017; Rasmussen et al., 2024)	untested beyond the first interglacial's detrital grains
Ice-free CO_2 from 253 (one Myr after the first deglaciation) down to 53 before the fourth entry (minima 52–66)	no	a paleosol dated to an ice-free interval between 2.43 and 2.24 Ga, analyzed with either barometer (Sheldon, 2006; Kanzaki and Murakami, 2015): weathering surfaces above the third Huronian glacial, the Hekpoort and Daspoort disconformities, the Turee Creek Group	not yet a test: the Ville Marie and Hokkalampi bands overlap the range, most central values below half its minimum; neither profile dated to an interglacial (Supplementary Text S8)
Deglaciation CO_2 238–281, drawn down about fourfold in each interval	no	cap-carbonate, weathering-intensity or triple-oxygen-isotope barometry above each diamictite; cap carbonates occur above the basal Duitschland diamictite (Gumsley et al., 2017)	untested; set by the assumed deglaciation level
Carbonate $\delta^{13}C$ −1.0 to −0.3 per mil before the first ice; step across the transition +0.29 per mil	no	compiled record: baseline within ±2 per mil before 2445 Ma; Lomagundi–Jatuli peak +7.3 per mil at 2130 Ma (Edmonsond and Dyer, 2026)	baseline is an input; the model has no mechanism for the excursion
Later O_2 6.3×10^{-5}–6.0×10^{-4} PAL, set by two prescribed post-transition schedules with no redox feedback	no	paleosol floor ≥0.14 PAL after the transition (Rye and Holland, 1998); paleosol weathering barometry (Kanzaki and Murakami, 2016); chromium ceiling $< 10^{-3}$ PAL, 1.8–0.85 Ga (Planavsky et al., 2014b)	floor missed by a factor 800 or more (comparison specified in advance; failed); barometer and ceiling met; tests the post-transition inputs, not the transition
Implied Marinoan duration 5.1 Myr, Sturtian 5.3 Myr, from the same sub-ice carbon rule	no	dated durations 4–15 and 57–59 Myr (Hoffman et al., 2017)	Marinoan met (the rule's one check); Sturtian not reproduced
Assumptions: $N_2 \geq 0.57$ bar; glaciation threshold ≤ 14.7 W m^{-2}; weathering e-folding temperature 6.6–19.6 K; emergence by 2.38 Ga; sub-ice anoxia; uptake of most of the carbon outgassed beneath the ice; the modern ocean–air partition β_w after each thaw	no	N_2 barometry through the transition (the one Neoarchean estimate is below half a bar; Som et al., 2016); a general circulation model at the transition's boundary conditions (Feulner et al., 2023); emergence chronologies (Kump and Barley, 2007; Bindeman et al., 2018); sub-glacial carbonate and altered-basalt archives (Hoffman et al., 2017)	untested; each would constrain one assumption (Section 4.5)

PRELIMINARY

cannot discriminate. Under the oxygen-only criterion of Pavlov and Kasting (2002) the model atmosphere permits the anomaly until early in the second interglacial, 15 Myr after the youngest onset of oxygenation that the Kaapvaal succession allows (2.368 Ga, the young age limit of the Mooidraai dolomite, tabulated as anomaly-free; Table 2) and 81 Myr after MIF-S disappears on Kola. Under the criterion of Zahnle et al. (2006), which also requires methane at the parts-per-million level, the anomaly ends when methane falls below that level, at 2.475 Ga, before the first ice and consistent with the Kola constraint. That date also precedes deposition of the anomaly-bearing Koegas Subgroup below the Makganyene diamictite (2440–2460 Ma; Senger et al., 2023), and because methane never again reaches 8 ppmv, none of the later returns to anoxia restores the anomaly under this criterion. The model thus fails in opposite directions under the two criteria, and we do not combine their outcomes. Under either criterion the model produces no oxygen pulse during deposition of the Hotazel Formation in the first interglacial, and it fails there if the cerium anomaly of that formation records oxygenation, as Gumsley et al. (2017) suggest (Table 2). Oxygen also stays far below the Huronian detrital-uraninite bound of that interglacial, reaching only about 0.03 times that bound.

4.4 Carbon dioxide, carbon isotopes and later oxygen

Before the first glaciation the modeled carbon dioxide lies between the two paleosol estimates, matching neither (Fig. 5b,e). Between the glaciations carbon dioxide stands one Myr after a deglaciation at 221–253 times pre-industrial and falls to 53–65 before the next glaciation, a prediction that a dated interglacial paleosol could test; the values just after a deglaciation inherit the assumed deglaciation level and sub-ice store, whereas the drawdown minima are the model's own. We applied both barometers to Ville Marie in Quebec (Panahi et al., 2000) and the porewater inversion to Hokkalampi in Finland (Marmo, 1992), the two profiles from the glacial era with suitable published chemistry. The resulting estimates overlap the modeled interglacial range, all but one central value lying below half of its minimum, but are not yet a test, because neither profile is dated to an interglacial and the mass-balance values assume a formation time (Supplementary Text S8).

Because the burial fraction is taken from the compilation of Krissansen-Totton et al. (2015), the modeled carbonate $\delta^{13}C$ reproduces that compilation before the first glaciation and equals its later-era means afterward. Across the transition it changes by +0.29 per mil where the carbonate record rises by about +7.9 (Edmonsond and Dyer, 2026), so the model does not reproduce the Lomagundi–Jatuli excursion. After the last deglaciation the model's oxygen level (6.3×10^{-5} PAL at 2.2 Ga, rising to 6.0×10^{-4} at 1.4 Ga) is set by the small excess of the flat burial flux over the declining isotope-inferred sink, two schedules with no redox feedback. The oxygen proxies therefore test these two prescribed inputs, and the level lies inside the paleosol weathering-barometer estimates and below the chromium-isotope ceiling (Table 2) but falls short of the paleosol floor (Rye and Holland, 1998) by a factor of 800 or more, a comparison specified in advance that the model fails. We attribute the shortfall, like the missing excursion, to the absence of an oxygen-overshoot mechanism and do not apply the model to oxygen after the last deglaciation.

4.5 The outgassing exponent and the model assumptions

Holding the other inputs at their Table 1 values, we find that the number of glaciations falls one at a time as ν rises above $\nu \simeq 0.55$ (Fig. 6). Where ν is too large for any glaciation (45% of the published range), oxygen rises once and smoothly, the single step of the textbook picture, and the Makganyene glaciation alone excludes these values. Of the published outgassing histories converted to this exponent, none lies within the four-glaciation interval, and because the nearest of them share the declining-heat-flow convention of our outgassing law, we do not take their closeness as independent support (Supplementary Text S2).

We varied the assumptions of Table 1 and the prescribed emergence date, singly and jointly, with ν fixed by the number of glaciations each time (Fig. 7). Three or four glaciations and none later occur at some ν for a glaciation threshold up to 14.7 $W\,m^{-2}$, nitrogen down to 0.57 bar, a weathering e-folding temperature of 6.6–19.6 K and emergence complete by 2.38 Ga. They also occur for sub-ice venting fractions up to a tenth and across the ranges of weathering response time, modern outgassing and, with one exception (Supplementary Text S4), deglaciation level. Sampling eight of these ranges jointly by Latin hypercube (with the sub-ice carbon partition in place of the venting fraction), we find such a ν in a fraction 0.45 of the samples (0.40–0.50 at 95% confidence).

At any one setting of the assumptions the glaciation count therefore fixes ν to about ± 0.015 (three or four glaciations; 2.1% of the published range at the Table 1 setting), and varying the assumptions moves that value over most of the published range: over the samples that have such a ν it has median 0.64 and central 90% range 0.22–0.98. With the threshold of Feulner et al. (2023) or half a bar of nitrogen adopted alone no ν gives the recorded glacial era, whereas in the joint sampling their opposite effects on ν partly compensate (Fig. 7b). Where no ν gives that era, weathering is most often too sensitive to temperature or emergence too late.

PRELIMINARY

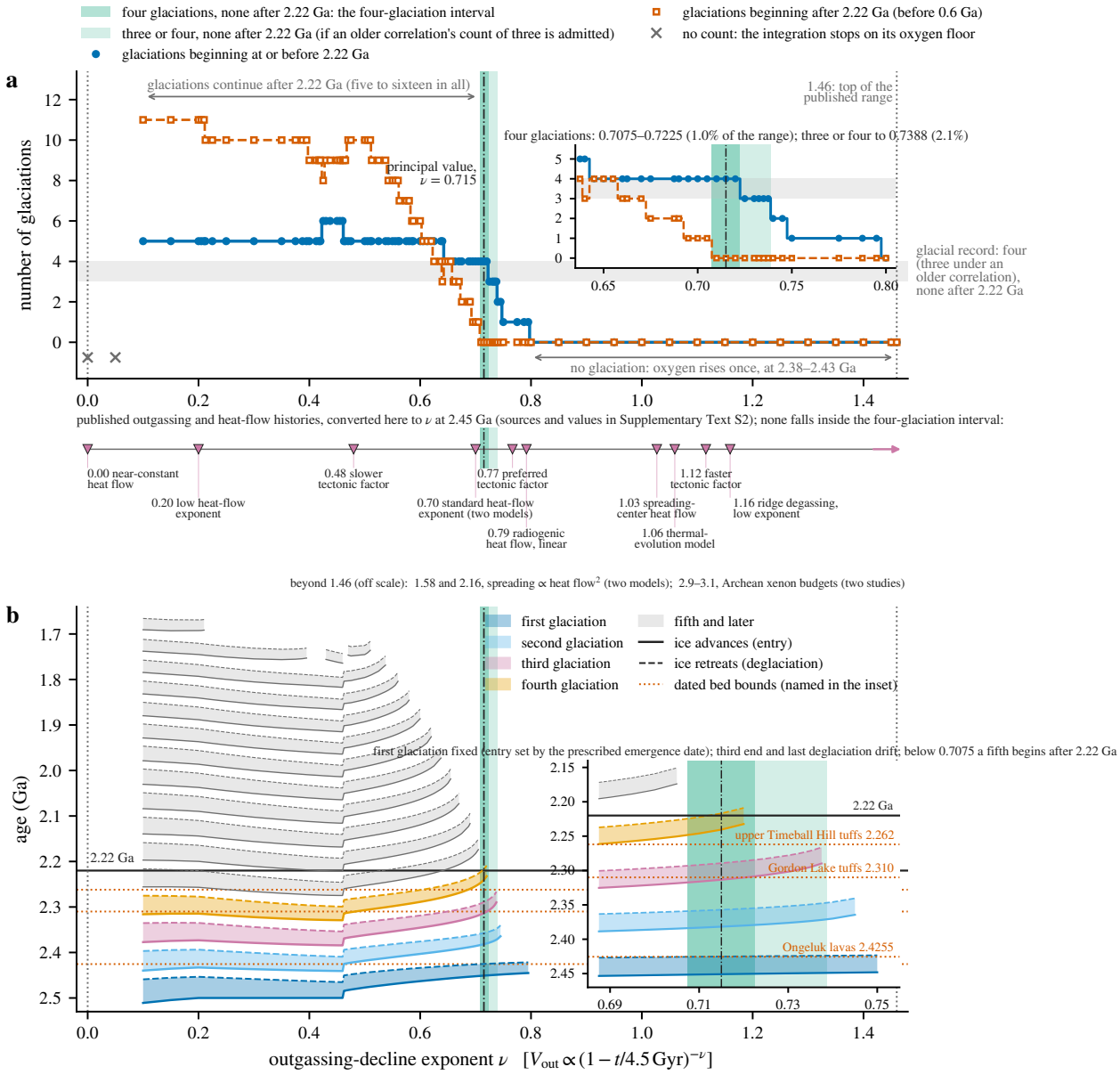

Figure 6: Number and timing of the model's Paleoproterozoic glaciations against the outgassing-decline exponent ν over the range sampled by Krissansen-Totton et al. (2018). (a) Number of glaciations beginning before and after 2.22 Ga, from exploratory calculations with the other inputs held at their Table 1 values. Above the four-glaciation interval the number falls one at a time as ν increases, until no glaciation occurs and oxygen rises once; below the interval, glaciations continue after 2.22 Ga. The strip below (a) shows published outgassing histories converted by us to ν at 2.45 Ga (Supplementary Text S2), of which none falls inside that interval. (b) Onset (solid) and deglaciation (dashed) ages of each glaciation with their dated bounds. Wherever three or four glaciations occur, the first spans the Ongeluk lava age, whereas the end of the third and the last deglaciation shift with ν. Four glaciations beginning by 2.22 Ga and none later occur only for $0.7075 < \nu < 0.7225$, 1.0% of the sampled range, and three or four only for ν up to 0.7388. The number of glaciations thus fixes ν, and Fig. 7 shows how the interval giving three or four glaciations shifts with the model's assumptions. In the methane-only case of Section 2.2 the edges of the four-glaciation interval move by no more than the spacing in ν of the points plotted in (a), and one glaciation still occurs up to $\nu = 0.839$ instead of 0.7975.

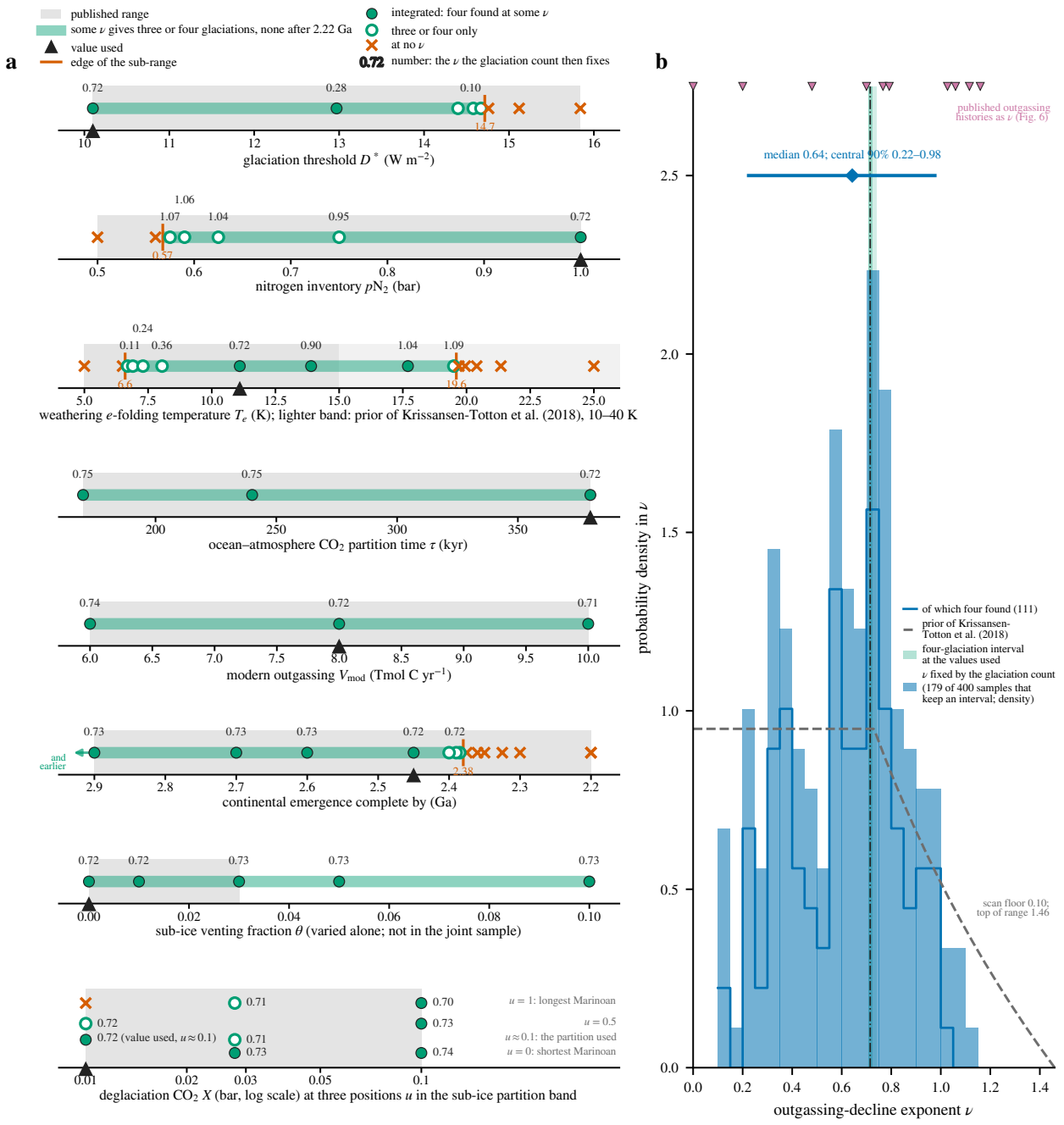

Figure 7: Sensitivity of the interval of ν fixed by the glaciation count to the model's assumptions and the prescribed emergence date, varied singly (a) and jointly (b). (a) For each of these inputs, the published range (gray), the value used (triangle) and the sub-range (green) in which some ν gives three or four glaciations by 2.22 Ga and none later. The sub-ranges have edges (orange ticks) at a glaciation threshold of 14.7 W m^{-2}, at 0.57 bar of nitrogen, at weathering e-folding temperatures of 6.6 and 19.6 K, and at emergence complete by 2.38 Ga. Symbols mark the values at which the model was integrated (filled, four glaciations at some ν; open, three or four only; cross, three or four at no ν). The number beside each circle is the calibrated ν, the center of the interval of ν over which three or four glaciations occur at that value of the input. Along the bars the calibrated ν takes values from 0.10 to 1.10. (b) Distribution of the calibrated ν over those of the 400 joint samples of eight ranges (venting varied singly; Supplementary Text S4) in which three or four glaciations occur at some ν (four rather than three in at least a fraction 0.28 of all samples). The prior of Krissansen-Totton et al. (2018) is drawn for comparison; 68% of it lies below the principal value, $\nu = 0.715$. The calibrated ν decreases with the glaciation threshold (-0.12 per W m^{-2}) and with the nitrogen inventory (-0.81 per bar), and a higher threshold and less nitrogen therefore shift it in opposite directions. The two shifts partly cancel, and 11 of the 21 joint samples with a threshold above 14.7 W m^{-2} and less than 0.6 bar of nitrogen still give three or four glaciations at some ν. The number of glaciations thus constrains ν narrowly at any one setting of the assumptions, whereas from one setting to another the calibrated value varies over most of the published range of ν.

The carbon taken up under the ice sets the glaciation length, 18.5–25.9 Myr across the sub-ice partitions consistent with the dated Marinoan duration and about 10 Myr with a calcite-saturation partition, and the carbon returned at the deglaciation sets the spacing. That spacing also assumes the returned carbon stays exchangeable at the modern open-water partition β_w; with a calcite-saturation partition instead, interglacials last 12 Myr at most. If the sub-ice carbon is instead sequestered in ocean crust (Le Hir et al., 2008), four glaciations of nearly the same length still occur, for $\nu = 0.719$–0.732 (Table 3). Their number is unchanged by crustal storage but their dates are not: inside that interval the Gordon Lake bound is met at the middle and the upper Timeball Hill tuffs near the upper edge, never both, and oxygenation still begins later than the Kaapvaal sulfur record allows (Supplementary Text S1). A dated glacial duration would therefore test the uptake and a dated spacing the return; the glaciation count, which fixes ν only once the sub-ice rule is chosen, tests neither.

5 Discussion

Our results suggest that, if volcanic outgassing declined as steeply as the Paleoproterozoic glaciations require in the model, and if oxygen and methane produced beneath the ice were consumed there with at most 3 percent vented, an episodic first rise of oxygen of the kind inferred by Poulton et al. (2021) follows from published photochemistry (Claire et al., 2006) and carbon-cycle laws (Krissansen-Totton et al., 2018) driven by dated inputs.

5.1 The stepwise view and prior work

Daines and Lenton (2016) argued for an episodic rise of oxygen before one was inferred from the Transvaal glacial and sulfur isotope records (Gumsley et al., 2017; Poulton et al., 2021). Earlier, Claire et al. (2006) obtained three successive glaciations in which "methane collapses and rises repeatedly" because their methane source depends on temperature, whereas ours follows the volcanic hydrogen supply. In our model methane collapses once, about thirty Myr before the first glaciation (twelve in the methane-only case of Section 2.2), and the loss of the remnant triggers that glaciation; the subsequent glaciations begin without methane and repeat the outgassing–weathering limit cycle of Tajika (2007).

Alcott et al. (2019) proposed an ocean–atmosphere model in which internal feedbacks convert a smooth decline in the reductant input into oxygenation steps. We solved the model exactly at the authors' published parameter values and find at most one stable equilibrium, a low-oxygen state on the pre-oxidation branch of their own steady-state diagram. At the reductant input of their Great Oxidation and the weakest burial feedbacks they consider, no oxygenated state coexists with it, so the network is not bistable there. Under the authors' declining input, at those feedbacks and at the stronger ones of their own simulations, its atmosphere oxygenates once and permanently, whereas a later version returns to anoxia in response to imposed post-glacial pulses (Alcott et al., 2026). The same analysis recovers both stable states of the Goldblatt et al. (2006) model (Supplementary Text S7).

5.2 Scope of the findings

The date of permanent oxygenation is unsettled between the estimate of Poulton et al. (2021) and older ones (Bekker et al., 2004; Luo et al., 2016). In the model, oxygen becomes permanent at the last deglaciation; its date, which follows from the glaciation count and the sub-ice treatment, falls on the younger estimate without deciding between them. The photochemistry sets the direction and sharpness of the transition, but because $t_\times$ is prescribed its timing comes from the rock record, as in other such models, and the model does not determine whether a rising oxygen source or a falling sink produced it.

The returns to anoxia during the glaciations follow from the sub-ice treatment, under which any gas vented through the ice is net reducing because oxygen from sub-ice burial cannot offset the continuing hydrogen supply. The air is oxic in every ice-free interval after 2.353 Ga, and without that treatment the glaciations would not interrupt the rise of oxygen. Under both criteria for preserving the MIF-S anomaly the model fails the comparison with the sulfur isotope record, in opposite directions (Section 4.3). It loses the anomaly too late for Kola under the oxygen-only criterion and too early for the Koegas Subgroup under the methane criterion, under which, because methane never recovers, its later returns to anoxia leave no isotopic trace. Each constraint is met under one criterion only, and the two successes cannot be combined. The model cannot resolve the conflict between the criteria, part of which lies in the rock record: on Kola the anomaly is lost at least 9.5 Myr before the youngest Makganyene glacial bed, beneath which it is still present on the Kaapvaal craton.

Our model omits the sulfur and iron cycles, carbonate chemistry, a spatially resolved ocean and any internal mechanism for the Lomagundi–Jatuli excursion or an oxygen overshoot, and we have not tested

PRELIMINARY

Table 3: The two sub-ice carbon storage cases against the dated beds. The tests of Table 2 are given under the adopted store, which is returned to the ocean–atmosphere system at each deglaciation, and under storage of the sub-ice carbon in altered ocean crust with only the airborne excess returned (Le Hir et al., 2008). With crustal storage four glaciations occur for $\nu = 0.719$–0.732 instead of 0.7075–0.7225 (Supplementary Text S1), and that case is shown at the middle and near the upper edge of this interval. In both cases the carbon exchangeable after a thaw is divided between air and ocean by the modern partition β_w; with crustal storage this division is made in a single step at the thaw, so that atmospheric CO_2 falls instantaneously (Supplementary Text S1). In each column ν lies in the interval fixed by the glaciation count of the first row (at its middle unless stated), so that row is calibration, as are the rows marked "count". Four glaciations of nearly the same length occur in both cases, but which dated beds are met differs between them and, under crustal storage, varies with ν inside its four-glaciation interval. In no column is every bed met: the adopted store misses the Gordon Lake bound, crustal storage at mid-interval meets that bound but misses the upper Timeball Hill tuffs and the open interval, and crustal storage near the upper edge meets the upper Timeball Hill, open-interval and Hekpoort bounds but misses the Gordon Lake and Makganyene ages by 2.0 and 2.5 Myr. If ν were set near that upper edge because those beds are met there, they would become calibration data like the first row and would no longer test the model. Both tests against the sulfur isotope record (the date of first oxic air and the end of the MIF-S anomaly) fail in all three columns. "Met by" and "missed" give the distance to the bound in Myr on its allowed or excluded side (for the Hekpoort window, to its nearer edge), with the direction of a miss (late, early, young, short). Ages in Ga; bed ages (Ma) carry 2σ uncertainties; CO_2 in multiples of pre-industrial.

	returned store (adopted), $\nu = 0.715$	crustal storage, $\nu = 0.725$ (mid-interval)	crustal storage, $\nu = 0.73125$ (near the upper edge)	dated bound (source)
Glaciations beginning by 2.22 Ga (later ones); durations; ice-free intervals (Myr)	four (none); 23.6–25.7; 43.4, 43.7, 48.8	four (none); 22.5–23.1; 33.0, 34.9, 38.9	four (none); 22.3–23.0; 35.4, 37.9, 51.4	four Paleoproterozoic glaciations and none later (Gumsley et al., 2017; Rasmussen et al., 2013): the calibration target in each column
First glaciation and the Ongeluk lavas	2.4509–2.4251: met, ice at the central age	2.4500–2.4269: met at 2σ; ice gone 1.4 Myr before the central age	2.4496–2.4266: met at 2σ; ice gone 1.1 Myr before the central age	lavas 2425.5 ± 2.6 Ma erupted into the ice (Gumsley et al., 2017); the start of this glaciation is prescribed
First glaciation, duration (Myr)	25.7: met by 5.4	23.1: met by 8.0	23.0: met by 8.1	at most 31.1, Heynskop to Ongeluk (Senger et al., 2023; Gumsley et al., 2017); on Kola at most 9 (Warke et al., 2020), missed in all three
First deglaciation and the Makganyene diamictite	2.4251: missed, 1.0 early	2.4269: missed, 2.8 early	2.4266: missed, 2.5 early	ice still present at 2.4241: diamictite MAK-D 2423.1 ± 1.0 Ma (Senger et al., 2023)
Third glaciation ends	2.289: missed, 20.7 late	2.313: met by 3.3	2.308: missed, 2.0 late	ice gone by 2.310: Gordon Lake tuffs (Rasmussen et al., 2024); lower Timeball Hill Re–Os and tuff ages (Hannah et al., 2004; Rasmussen et al., 2013)
Fourth glaciation begins	2.2405: met by 21.5	2.2745: missed, 12.5 early	2.2566: met by 5.4	after 2.262: upper Timeball Hill tuffs below the Rietfontein diamictite (Rasmussen et al., 2013)
Open water between the third and fourth glaciations (Myr; count)	48.8: met by 0.8	38.9: missed, 9.1 short	51.4: met by 3.4	at least 48 of open-marine Timeball Hill shale (Hannah et al., 2004; Rasmussen et al., 2013)
Last deglaciation (count)	2.217: missed, 3.1 young	2.252: met by 4.0	2.234: met by 14.3	2.256–2.220: Hekpoort lava above the Rietfontein, 2247 ± 20 Ma, age model (Schröder et al., 2016)
Permanent oxygenation, t_{perm} (count)	2.217, the last deglaciation	2.252, the same	2.234, the same	estimates 2.22 (Poulton et al., 2021) and 2.33–2.32 (Luo et al., 2016; Bekker et al., 2004); set by the glaciation count and the sub-ice treatment, not a test
First oxic air ($\geq 10^{-5}$ PAL), oxygen-only criterion (Pavlov and Kasting, 2002)	2.353, 4 Myr after the second deglaciation: late by 15 (Kaapvaal), 81 (Kola)	2.358, 13 Myr after it: late by 10, 76	2.360, 8 Myr after it: late by 8, 73	anomaly lost by 2.368 on the Kaapvaal craton (Mooidraai dolomite; Gumsley et al., 2017) and by 2.4336 on Kola (Warke et al., 2020); the first interglacial is anoxic in all three
End of the MIF-S anomaly, methane criterion (Zahnle et al., 2006)	2.475 (2.458 in the methane-only case), before the first ice: Kola met; Koegas missed, no return	2.474: the same	2.474: the same	anomaly kept while $CH_4 \geq 8$ ppmv: lost on Kola by 2.4336; still present in the Koegas Subgroup, 2440–2460 Ma (Senger et al., 2023)
Ice-free CO_2: one Myr after the first deglaciation → minimum before the fourth glaciation	253 → 53	114 → 56	116 → 54	not yet a test: the paleosol estimates overlap either range (Supplementary Text S8); the value after a thaw inherits the assumed deglaciation level and returned share

PRELIMINARY

its response to stochastic outgassing. It describes the transition only; afterward its oxygen follows from two prescribed schedules (Section 4.4). Imposed as excess organic burial, the excursion mostly preserves the glaciation count if its carbon is marine and the released oxygen reaches the air, and otherwise adds or removes glaciations; the isotopes determine neither condition (Supplementary Text S5).

We assume that the methane source G is hydrogenotrophic, made from volcanic hydrogen. With R_A prescribed and G_A set by $t_\times$, the reading of R and G as two draws on one hydrogen supply, which justifies their common shape and which we owe to D. T. Johnston, is consistent with the model rather than derived by it. Hydrogen escape adds no oxygen to the instantaneous atmospheric balance, but in the long-term planetary budget (Catling et al., 2001) it leaves behind oxidizing power, 0.69–1.19 times the surface oxidant inventory of Hayes and Waldbauer (2006), for which the model has no crustal or mantle reservoir. The model therefore leaves open whether declining methanogenesis delayed oxidation by slowing hydrogen loss, as Kasting (2013) argued. The question was put by D. T. Johnston, and the distinction between the long-term planetary budget and the instantaneous atmospheric balance is his.

5.3 Tests of the model

Table 2 lists measurements that would test the model's dated statements and inputs. The most decisive would be an age precise to a few Myr for the Rooihoogte or Gowganda contact marking the end of the third glaciation, when the model is still glaciated. An interglacial paleosol dated between 2.43 and 2.24 Ga and analyzed with either CO_2 barometer would test the model's carbon cycle, and a value below about half its interglacial minimum or above its post-glacial maximum would count against it. A dated glacial duration or spacing would test the sub-ice carbon store, which the glaciation count does not. Because ν was fixed in part by the absence of later glaciation, a glacial deposit or a renewed MIF-S anomaly above the Hekpoort lava would contradict the model.

6 Conclusions

With the outgassing decline fixed by the glacial record and with the other inputs published, prescribed or assumed, our model's Great Oxidation spans four snowball glaciations between 2.45 and 2.22 Ga. By assumption each glaciation returns the air to anoxia; oxic air first appears at 2.35 Ga, later than the sulfur isotopes allow under the oxygen-only criterion. The first glaciation, whose start is prescribed, spans the Ongeluk lava age, and the fourth begins after the upper Timeball Hill tuffs, two agreements that do not follow from the glaciation count. The third glaciation, however, ends about 20 Myr later than the Gordon Lake tuffs allow (with the adopted sub-ice carbon store; Table 3), and the model reproduces neither the Lomagundi–Jatuli excursion nor the post-transition paleosol oxygen level.

These glaciations require uptake, though not return, of most of the carbon outgassed beneath the ice and, with the other assumptions unchanged, continental emergence complete by 2.38 Ga, at least 0.57 bar of nitrogen (about one bar for four glaciations) and nearly the lowest published glaciation threshold. Their spacing also assumes the returned carbon stays exchangeable at the modern ocean partition. In the model the Great Oxidation is an oscillation paced by the glaciations, with no periodic forcing, and oxygen becomes permanent when the brightening Sun ends the glacial era.

Acknowledgments

Funding for this project was provided by Anthropic. This is not an official Anthropic project and results and views are not endorsed by Anthropic.

Data availability

The model code, the input tables, the model output underlying each figure and table, and the code and interval-arithmetic output of the steady-state enumerations of Supplementary Text S7 accompany this submission as a supplementary archive and will be deposited in a public repository, with a DOI added here, on acceptance. The geological data used to test the model are taken from the sources cited in the text and are tabulated with those sources in the Supplementary Material.

PRELIMINARY

References

D. S. Abbot, A. Voigt, M. Branson, R. T. Pierrehumbert, D. Pollard, G. Le Hir, and D. D. B. Koll. Clouds and Snowball Earth deglaciation. *Geophysical Research Letters*, 39(20):L20711, 2012. doi: 10.1029/2012GL052861.

L. J. Alcott, B. J. W. Mills, and S. W. Poulton. Stepwise Earth oxygenation is an inherent property of global biogeochemical cycling. *Science*, 366(6471):1333–1337, 2019. doi: 10.1126/science.aax6459.

L. J. Alcott, B. J. W. Mills, A. Bekker, Z. Peng, and S. W. Poulton. A nutrient control on oxygenation dynamics during Earth's Great Oxidation Episode. *Nature Communications*, 2026. doi: 10.1038/s41467-026-76597-y. published online 27 August 2026.

A. D. Anbar, Y. Duan, T. W. Lyons, G. L. Arnold, B. Kendall, R. A. Creaser, A. J. Kaufman, G. W. Gordon, C. Scott, J. Garvin, and R. Buick. A whiff of oxygen before the Great Oxidation Event? *Science*, 317: 1903–1906, 2007. doi: 10.1126/science.1140325.

A. Bekker, H. D. Holland, P.-L. Wang, D. Rumble III, H. J. Stein, J. L. Hannah, L. L. Coetzee, and N. J. Beukes. Dating the rise of atmospheric oxygen. *Nature*, 427:117–120, 2004. doi: 10.1038/nature02260.

N. J. Beukes and S. Schröder. Sedimentary and stratigraphic architecture of the Duitschland and Rooihoogte formations (Palaeoproterozoic, South Africa): implications for tempo of the Great Oxidation Event. *South African Journal of Geology*, 127(2):433–454, 2024. doi: 10.25131/sajg.127.0006.

I. N. Bindeman, D. O. Zakharov, J. Palandri, N. D. Greber, N. Dauphas, G. J. Retallack, A. Hofmann, J. S. Lackey, and A. Bekker. Rapid emergence of subaerial landmasses and onset of a modern hydrologic cycle 2.5 billion years ago. *Nature*, 557:545–548, 2018. doi: 10.1038/s41586-018-0131-1.

A. T. Brasier, A. P. Martin, V. A. Melezhik, A. R. Prave, D. J. Condon, and A. E. Fallick. Earth's earliest global glaciation? Carbonate geochemistry and geochronology of the Polisarka Sedimentary Formation, Kola Peninsula, Russia. *Precambrian Research*, 235:278–294, 2013. doi: 10.1016/j.precamres.2013.06.007.

B. Byrne and C. Goldblatt. Radiative forcings for 28 potential Archean greenhouse gases. *Climate of the Past*, 10(5):1779–1801, 2014. doi: 10.5194/cp-10-1779-2014.

D. C. Catling, K. J. Zahnle, and C. P. McKay. Biogenic methane, hydrogen escape, and the irreversible oxidation of early Earth. *Science*, 293(5531):839–843, 2001. doi: 10.1126/science.1061976.

M. W. Claire, D. C. Catling, and K. J. Zahnle. Biogeochemical modelling of the rise in atmospheric oxygen. *Geobiology*, 4(4):239–269, 2006. doi: 10.1111/j.1472-4669.2006.00084.x.

G. Colbourn, A. Ridgwell, and T. M. Lenton. The time scale of the silicate weathering negative feedback on atmospheric CO_2. *Global Biogeochemical Cycles*, 29(5):583–596, 2015. doi: 10.1002/2014GB005054.

S. J. Daines and T. M. Lenton. The effect of widespread early aerobic marine ecosystems on methane cycling and the Great Oxidation. *Earth and Planetary Science Letters*, 434:42–51, 2016. doi: 10.1016/j.epsl.2015.11.021.

S. G. Driese, M. A. Jirsa, M. Ren, S. L. Brantley, N. D. Sheldon, D. Parker, and M. Schmitz. Neoarchean paleoweathering of tonalite and metabasalt: Implications for reconstructions of 2.69 Ga early terrestrial ecosystems and paleoatmospheric chemistry. *Precambrian Research*, 189(1-2):1–17, 2011. doi: 10.1016/j.precamres.2011.04.003.

S. Edmonsond and B. Dyer. Timing and magnitude of the Lomagundi–Jatuli carbon isotope excursion. *Proceedings of the National Academy of Sciences*, 123(2):e2512767123, 2026. doi: 10.1073/pnas.2512767123.

D. A. Evans, N. J. Beukes, and J. L. Kirschvink. Low-latitude glaciation in the Palaeoproterozoic era. *Nature*, 386:262–266, 1997. doi: 10.1038/386262a0.

J. Farquhar, H. Bao, and M. Thiemens. Atmospheric influence of Earth's earliest sulfur cycle. *Science*, 289: 756–758, 2000. doi: 10.1126/science.289.5480.756.

G. Feulner, M. Bukenberger, and S. Petri. Tracing the Snowball bifurcation of aquaplanets through time reveals a fundamental shift in critical-state dynamics. *Earth System Dynamics*, 14(3):533–547, 2023. doi: 10.5194/esd-14-533-2023.

PRELIMINARY

C. Goldblatt, T. M. Lenton, and A. J. Watson. Bistability of atmospheric oxygen and the Great Oxidation. *Nature*, 443(7112):683–686, 2006. doi: 10.1038/nature05169.

D. O. Gough. Solar interior structure and luminosity variations. *Solar Physics*, 74:21–34, 1981. doi: 10.1007/BF00151270.

A. P. Gumsley, K. R. Chamberlain, W. Bleeker, U. Söderlund, M. O. de Kock, E. R. Larsson, and A. Bekker. Timing and tempo of the Great Oxidation Event. *Proceedings of the National Academy of Sciences*, 114:1811–1816, 2017. doi: 10.1073/pnas.1608824114.

I. Halevy, D. T. Johnston, and D. P. Schrag. Explaining the structure of the Archean mass-independent sulfur isotope record. *Science*, 329(5988):204–207, 2010. doi: 10.1126/science.1190298.

J. L. Hannah, A. Bekker, H. J. Stein, R. J. Markey, and H. D. Holland. Primitive Os and 2316 Ma age for marine shale: implications for Paleoproterozoic glacial events and the rise of atmospheric oxygen. *Earth and Planetary Science Letters*, 225(1-2):43–52, 2004. doi: 10.1016/j.epsl.2004.06.013.

M. Harada, E. Tajika, and Y. Sekine. Transition to an oxygen-rich atmosphere with an extensive overshoot triggered by the Paleoproterozoic snowball Earth. *Earth and Planetary Science Letters*, 419:178–186, 2015. doi: 10.1016/j.epsl.2015.03.005.

J. C. Havsteen, I. C. Kleinhanns, S. Schröder, B. Eickmann, G. Izon, M. D. Gogouvitis, R. Ngobeli, N. J. Beukes, and R. Schoenberg. Evidence for contemporaneous deposition of the Duitschland and Rooihoogte formations (Transvaal Supergroup): Implications for tempo and mode of Earth's Great Oxidation. *Precambrian Research*, 391:107055, 2023. doi: 10.1016/j.precamres.2023.107055.

J. M. Hayes and J. R. Waldbauer. The carbon cycle and associated redox processes through time. *Philosophical Transactions of the Royal Society B*, 361(1470):931–950, 2006. doi: 10.1098/rstb.2006.1840.

P. F. Hoffman, D. S. Abbot, Y. Ashkenazy, D. I. Benn, J. J. Brocks, P. A. Cohen, G. M. Cox, J. R. Creveling, Y. Donnadieu, D. H. Erwin, I. J. Fairchild, D. Ferreira, J. C. Goodman, G. P. Halverson, M. F. Jansen, G. Le Hir, G. D. Love, F. A. Macdonald, A. C. Maloof, C. A. Partin, G. Ramstein, B. E. J. Rose, C. V. Rose, P. M. Sadler, E. Tziperman, A. Voigt, and S. G. Warren. Snowball Earth climate dynamics and Cryogenian geology-geobiology. *Science Advances*, 3:e1600983, 2017. doi: 10.1126/sciadv.1600983.

H. D. Holland. Volcanic gases, black smokers, and the great oxidation event. *Geochimica et Cosmochimica Acta*, 66:3811–3826, 2002. doi: 10.1016/S0016-7037(02)00950-X.

J. E. Johnson, A. Gerpheide, M. P. Lamb, and W. W. Fischer. O_2 constraints from Paleoproterozoic detrital pyrite and uraninite. *Geological Society of America Bulletin*, 126(5-6):813–830, 2014. doi: 10.1130/B30949.1.

Y. Kanzaki and T. Murakami. Estimates of atmospheric CO_2 in the Neoarchean–Paleoproterozoic from paleosols. *Geochimica et Cosmochimica Acta*, 159:190–219, 2015. doi: 10.1016/j.gca.2015.03.011.

Y. Kanzaki and T. Murakami. Estimates of atmospheric O_2 in the Paleoproterozoic from paleosols. *Geochimica et Cosmochimica Acta*, 174:263–290, 2016. doi: 10.1016/j.gca.2015.11.022.

J. A. Karhu and H. D. Holland. Carbon isotopes and the rise of atmospheric oxygen. *Geology*, 24:867–870, 1996. doi: 10.1130/0091-7613(1996)024⟨0867:CIATRO⟩2.3.CO;2.

J. F. Kasting. What caused the rise of atmospheric O_2? *Chemical Geology*, 362:13–25, 2013. doi: 10.1016/j.chemgeo.2013.05.039.

P. Kharecha, J. Kasting, and J. Siefert. A coupled atmosphere–ecosystem model of the early Archean Earth. *Geobiology*, 3(2):53–76, 2005. doi: 10.1111/j.1472-4669.2005.00049.x.

K. O. Konhauser, E. Pecoits, S. V. Lalonde, D. Papineau, E. G. Nisbet, M. E. Barley, N. T. Arndt, K. Zahnle, and B. S. Kamber. Oceanic nickel depletion and a methanogen famine before the Great Oxidation Event. *Nature*, 458:750–753, 2009. doi: 10.1038/nature07858.

K. O. Konhauser, L. J. Robbins, E. Pecoits, C. Peacock, A. Kappler, and S. V. Lalonde. The Archean nickel famine revisited. *Astrobiology*, 15(10):804–815, 2015. doi: 10.1089/ast.2015.1301.

R. E. Kopp, J. L. Kirschvink, I. A. Hilburn, and C. Z. Nash. The Paleoproterozoic snowball Earth: A climate disaster triggered by the evolution of oxygenic photosynthesis. *Proceedings of the National Academy of Sciences*, 102:11131–11136, 2005. doi: 10.1073/pnas.0504878102.

PRELIMINARY

J. Krissansen-Totton and D. C. Catling. Constraining climate sensitivity and continental versus seafloor weathering using an inverse geological carbon cycle model. *Nature Communications*, 8:15423, 2017. doi: 10.1038/ncomms15423.

J. Krissansen-Totton, R. Buick, and D. C. Catling. A statistical analysis of the carbon isotope record from the Archean to Phanerozoic and implications for the rise of oxygen. *American Journal of Science*, 315(4): 275–316, 2015. doi: 10.2475/04.2015.01.

J. Krissansen-Totton, G. N. Arney, and D. C. Catling. Constraining the climate and ocean pH of the early Earth with a geological carbon cycle model. *Proceedings of the National Academy of Sciences*, 115(16): 4105–4110, 2018. doi: 10.1073/pnas.1721296115.

L. R. Kump and M. E. Barley. Increased subaerial volcanism and the rise of atmospheric oxygen 2.5 billion years ago. *Nature*, 448:1033–1036, 2007. doi: 10.1038/nature06058.

T. A. Laakso and D. P. Schrag. Regulation of atmospheric oxygen during the Proterozoic. *Earth and Planetary Science Letters*, 388:81–91, 2014. doi: 10.1016/j.epsl.2013.11.049.

T. A. Laakso and D. P. Schrag. A theory of atmospheric oxygen. *Geobiology*, 15(3):366–384, 2017. doi: 10.1111/gbi.12230.

G. Le Hir, Y. Goddéris, Y. Donnadieu, and G. Ramstein. A geochemical modelling study of the evolution of the chemical composition of seawater linked to a "snowball" glaciation. *Biogeosciences*, 5(1):253–267, 2008. doi: 10.5194/bg-5-253-2008.

G. Luo, S. Ono, N. J. Beukes, D. T. Wang, S. Xie, and R. E. Summons. Rapid oxygenation of Earth's atmosphere 2.33 billion years ago. *Science Advances*, 2(5):e1600134, 2016. doi: 10.1126/sciadv.1600134.

J. S. Marmo. The Lower Proterozoic Hokkalampi paleosol in North Karelia, eastern Finland. In *Early Organic Evolution*, pages 41–66. Springer, 1992. doi: 10.1007/978-3-642-76884-2_5.

B. Mills, A. J. Watson, C. Goldblatt, R. Boyle, and T. M. Lenton. Timing of Neoproterozoic glaciations linked to transport-limited global weathering. *Nature Geoscience*, 4(12):861–864, 2011. doi: 10.1038/ngeo1305.

C. Minsky, R. Wordsworth, D. T. Johnston, and A. H. Knoll. Repeated snowball–hothouse cycles within the Neoproterozoic Sturtian glaciation. *Proceedings of the National Academy of Sciences*, 123(19):e2525919123, 2026. doi: 10.1073/pnas.2525919123.

A. Panahi, G. M. Young, and R. H. Rainbird. Behavior of major and trace elements (including REE) during Paleoproterozoic pedogenesis and diagenetic alteration of an Archean granite near Ville Marie, Québec, Canada. *Geochimica et Cosmochimica Acta*, 64:2199–2220, 2000. doi: 10.1016/S0016-7037(99)00420-2.

A. A. Pavlov and J. F. Kasting. Mass-independent fractionation of sulfur isotopes in Archean sediments: strong evidence for an anoxic Archean atmosphere. *Astrobiology*, 2:27–41, 2002. doi: 10.1089/153110702753621321.

A. A. Pavlov, J. F. Kasting, L. L. Brown, K. A. Rages, and R. Freedman. Greenhouse warming by CH_4 in the atmosphere of early Earth. *Journal of Geophysical Research: Planets*, 105:11981–11990, 2000. doi: 10.1029/1999JE001134.

N. J. Planavsky, D. Asael, A. Hofmann, C. T. Reinhard, S. V. Lalonde, A. Knudsen, X. Wang, F. Ossa Ossa, E. Pecoits, A. J. B. Smith, N. J. Beukes, A. Bekker, T. M. Johnson, K. O. Konhauser, T. W. Lyons, and O. J. Rouxel. Evidence for oxygenic photosynthesis half a billion years before the Great Oxidation Event. *Nature Geoscience*, 7:283–286, 2014a. doi: 10.1038/ngeo2122.

N. J. Planavsky, C. T. Reinhard, X. Wang, D. Thomson, P. McGoldrick, R. H. Rainbird, T. Johnson, W. W. Fischer, and T. W. Lyons. Low mid-Proterozoic atmospheric oxygen levels and the delayed rise of animals. *Science*, 346:635–638, 2014b. doi: 10.1126/science.1258410.

S. W. Poulton, A. Bekker, V. M. Cumming, A. L. Zerkle, D. E. Canfield, and D. T. Johnston. A 200-million-year delay in permanent atmospheric oxygenation. *Nature*, 592(7853):232–236, 2021. doi: 10.1038/s41586-021-03393-7.

B. Rasmussen, A. Bekker, and I. R. Fletcher. Correlation of Paleoproterozoic glaciations based on U-Pb zircon ages for tuff beds in the Transvaal and Huronian Supergroups. *Earth and Planetary Science Letters*, 382:173–180, 2013. doi: 10.1016/j.epsl.2013.08.037.

PRELIMINARY

B. Rasmussen, J.-W. Zi, and A. Bekker. New U-Pb zircon tuff ages and revised stratigraphic correlations in the Superior craton during the Great Oxidation Episode. *Earth and Planetary Science Letters*, 640: 118779, 2024. doi: 10.1016/j.epsl.2024.118779.

R. Rye and H. D. Holland. Paleosols and the evolution of atmospheric oxygen: a critical review. *American Journal of Science*, 298:621–672, 1998. doi: 10.2475/ajs.298.8.621.

S. Schröder, N. J. Beukes, and R. A. Armstrong. Detrital zircon constraints on the tectonostratigraphy of the Paleoproterozoic Pretoria Group, South Africa. *Precambrian Research*, 278:362–393, 2016. doi: 10.1016/j.precamres.2016.03.016.

M. H. Senger, J. H. F. L. Davies, M. Ovtcharova, N. Beukes, A. Gumsley, S. P. Gaynor, A. Ulianov, R. Ngobeli, and U. Schaltegger. Improving the chronostratigraphic framework of the Transvaal Supergroup (South Africa) through in-situ and high-precision U-Pb geochronology. *Precambrian Research*, 392:107070, 2023. doi: 10.1016/j.precamres.2023.107070.

N. D. Sheldon. Precambrian paleosols and atmospheric CO_2 levels. *Precambrian Research*, 147:148–155, 2006. doi: 10.1016/j.precamres.2006.02.004.

S. P. Slotznick, J. E. Johnson, B. Rasmussen, T. D. Raub, S. M. Webb, J.-W. Zi, J. L. Kirschvink, and W. W. Fischer. Reexamination of 2.5-Ga "whiff" of oxygen interval points to anoxic ocean before GOE. *Science Advances*, 8(1):eabj7190, 2022. doi: 10.1126/sciadv.abj7190.

S. M. Som, R. Buick, J. W. Hagadorn, T. S. Blake, J. M. Perreault, J. P. Harnmeijer, and D. C. Catling. Earth's air pressure 2.7 billion years ago constrained to less than half of modern levels. *Nature Geoscience*, 9(6):448–451, 2016. doi: 10.1038/ngeo2713.

E. Tajika. Long-term stability of climate and global glaciations throughout the evolution of the Earth. *Earth, Planets and Space*, 59(4):293–299, 2007. doi: 10.1186/BF03353107.

B. T. Uveges, G. Izon, S. Ono, N. J. Beukes, and R. E. Summons. Reconciling discrepant minor sulfur isotope records of the Great Oxidation Event. *Nature Communications*, 14:279, 2023. doi: 10.1038/s41467-023-35820-w.

A. Voigt, D. S. Abbot, R. T. Pierrehumbert, and J. Marotzke. Initiation of a Marinoan Snowball Earth in a state-of-the-art atmosphere-ocean general circulation model. *Climate of the Past*, 7(1):249–263, 2011. doi: 10.5194/cp-7-249-2011.

M. R. Warke, T. Di Rocco, A. L. Zerkle, A. Lepland, A. R. Prave, A. P. Martin, Y. Ueno, D. J. Condon, and M. W. Claire. The Great Oxidation Event preceded a Paleoproterozoic "snowball Earth". *Proceedings of the National Academy of Sciences*, 117:13314–13320, 2020. doi: 10.1073/pnas.2003090117.

K. Zahnle, M. Claire, and D. Catling. The loss of mass-independent fractionation in sulfur due to a Palaeoproterozoic collapse of atmospheric methane. *Geobiology*, 4:271–283, 2006. doi: 10.1111/j.1472-4669.2006.00085.x.

PRELIMINARY